PONTIFICIA UNIVERSIDAD CATOLICA DE CHILE
ESCUELA DE INGENIERIA

CELL RESPONSE TO LOW-FREQUENCY MAGNETIC ROTATION OF Pt-Ni COMPOSITE NANORODS INCORPORATED INTO NIH/3T3 FIBROBLASTS

VALENTINA B. FRENKEL

Thesis submitted to the Office of Research and Graduate Studies in partial fulfillment of the requirements for the Degree of Master of Science in Engineering

Advisor:
LORETO VALENZUELA
DANIEL HURTADO

Santiago de Chile, August, 2017

© 2017, Valentina Frenkel

PONTIFICIA UNIVERSIDAD CATOLICA DE CHILE
ESCUELA DE INGENIERIA

CELL RESPONSE TO LOW-FREQUENCY MAGNETIC ROTATION OF Pt-Ni COMPOSITE NANORODS INCORPORATED INTO NIH/3T3 FIBROBLASTS

VALENTINA B. FRENKEL

Members of the Committee:

LORETO VALENZUELA

DANIEL HURTADO

TOMÁS EGAÑA

HUGO OLGUÍN

JORGE GIRONÁS

Thesis submitted to the Office of Research and Graduate Studies in partial fulfillment of the requirements for the Degree of Master of Science in Engineering

Santiago de Chile, August, 2017

To my family and friends, who inspired me, were my rocks and lighted a fire in me.

ACKNOWLEDGMENTS

I want to thank to my advisors, Loreto Valenzuela and Daniel Hurtado, for their guidance during my master's research. To Graciela Bravo for her collaboration through experimental design and execution of the experiments. To Hugo Olguín and his laboratory for their guidance and collaboration during the microtubule and nucleus labeling. To Matías Castillo for the nanorods fabrication guidance and Rodrigo del Río and Judy Castillo for the collaboration at their actual fabrication. To the laboratory of Biomaterials and Biopolymers for they advise about experimental considerations. To Mauricio Sarabia for his help measuring the magnetic field. To Alfredo Celedón who offered me the opportunity of participating in this project. To my beloved Cristhian Vásquez who supported me every day. To my friends, Magdalena Ribbeck, Ilenne del Valle, Min Bag and Hernan Gonzales for them advises on the manuscript, and Diego Bertín who helped me to transport a nitrogen tank from one university campus to other. I acknowledge the support of Pontifical Catholic University of Chile through grant the interdisciplinary research project CIEN-UC.

TABLE OF CONTENTS

Page

LIST OF TABLES

Page

LIST OF FIGURES

Page

RESUMEN

Nanocilindros magnéticos pueden incorporarse dentro de células para manipularlas usando campos magnéticos externos, deformando estructuras intracelulares y membrana celular, con el objetivo de inducir la muerte celular. Sin embargo, nanopartículas ferromagnéticas tienden a aglomerarse antes de ser insertadas en las células, formando una dispersión no homogénea que impide la incorporación celular y que genera efectos citotóxicos. En este trabajo se evalúa la factibilidad de usar nanocilindros magnéticos compuestos de Ni-Pt para la manipulación celular, estudiando los efectos mecánicos y biológicos que generan al insertase y rotar magnéticamente a baja frecuencia dentro de fibroblastos.

Como resultado, los nanocilindros de Ni-Pt mostraron mejores propiedades de dispersión que nanocilindros magnéticos de un solo material, ya que requieren menores tiempos de sonicación y presentan menos aglomeraciones. Los nanocilindros se incorporaron exitosamente en el citoplasma de cultivos celulares de fibroblastos NIH/3T3 y rotaron al aplicar un campo magnético rotatorio. Este tratamiento dañó la integridad de la membrana celular sólo cuando los nanocilindros y el campo magnético se aplicaron en conjunto. Por otro lado, los nanocilindros afectaron el funcionamiento normal de las células al inhibir la proliferación celular de forma dosis y tiempo dependiente, y al cambiar la morfología celular.

Así, se demostró que la incorporación de Pt en la composición de nanocilindros magnéticos de Ni mejora sus propiedades de homogenización. La pérdida de integridad de membrana, luego de un corto reposo tras realizar el tratamiento, indica muerte celular necrótica. Dado a que ni la presencia de los nanocilindros ni del campo magnético afectó la integridad de membrana por sí mismos, se concluye que las fuerzas que ejercen los nanocilindros contra las estructuras celulares producen daño mecánico. Además, los nanocilindros de Ni-Pt mostraron tener un efecto citostático en fibroblastos NIH/3T3, al dañar su funcionamiento normal. Con este trabajo se contribuye al entendimiento de nanocilindros de Ni-Pt, de sus ventajas de dispersión y efecto biológico.

Palabras Claves: Nanopartículas magnéticas, nanocilindros, fibroblastos NIH/3T3, campo magnético rotatorio, daño celular, integridad de membrana celular, microtúbulos.

ABSTRACT

Magnetic nanocylinders such as nanorods and nanowires have been inserted inside cells and mechanically manipulated by external magnetic fields in order to deform cytoplasmic structures and the cellular membrane, with the ultimate goal of inducing cell death. However, magnetic particles entirely made of ferromagnetic materials tend to aggregate before their insertion, resulting in a non-homogenous dispersion that prevents the cell uptake and increases the cytotoxic effect.

We assessed the feasibility of composite Ni-Pt magnetic nanorods by studying the associated mechanical and biological consequences when inserted into cells and subject to rotating magnetic fields. Ni-Pt composite nanorods were fabricated by electrochemical deposition and characterized by Atomic Force Microscopy and Scanning Electron Microscope. They display enhanced dispersion properties, as sonication times and the aggregation effect are smaller than those observed in single-material magnetic nanorods. Ni-Pt nanorods were effectively incorporated into the cytoplasm of NIH/3T3 fibroblast cells in culture and then subjected to low-frequency rotating magnetic field. We further confirm that such Ni-Pt nanorod magnetic treatment damages cell viability. Ni-Pt nanorods inhibit cellular proliferation and alter cell morphology, showing a dose-dependent and time-dependent cytotoxicity.

The observed cell membrane integrity damage indicates a necrotic cell death. Neither the nanorod presence nor the magnetic field affected the cell membrane by itself, indicating that mechanical damage is generated by nanorods torque exerting forces on intracellular structures. Additionally, Ni-Pt nanorods presence inhibits NIH/3T3 fibroblast cell proliferation, showing a cytostatic effect.

Keywords: Magnetic nanoparticles, nanorods, NIH/3T3 fibroblasts, rotating magnetic field, cellular damage, cell death, microtubules.

1. INTRODUCTION

Artificial cell manipulation has been studied for diagnostic, treatment and as a scientific tool. There are techniques that allow manipulating cells at micrometric and nanometric scales, as atomic force microscopy (AFM), and optical and magnetic tweezers (Gardel, Kasza, Brangwynne, Liu, & Weitz, 2008), but they can only act in one point at the time and cannot be used inside cells. In recent years, the use of magnetic nanoparticles (NPs) allows the manipulation of cells and their components, overcoming the limitations of AFM and tweezers.

1.1 Cell Manipulation by Magnetic Nanoparticles

Magnetic NPs had been fabricated and used to control cells when manipulated by an external magnetic field (MF). They can be fabricated with different shapes and compositions, which define their biocompatibility, mechanical and magnetic properties, and their colloidal stability. Spherical and cylindrical ferromagnetic NPs of different sizes have been incorporated inside cells (Castillo et al., 2014; Liao et al., 2015). NPs can be active targeting by specific molecular binding (Figure 1-1), passive targeting by physical mechanisms based on NP size, or targeting by localized physical forces such as MF that direct magnetic NPs to the desired body region (Sunderland, Steiert, Talmadge, Derfus, & Barry, 2006).

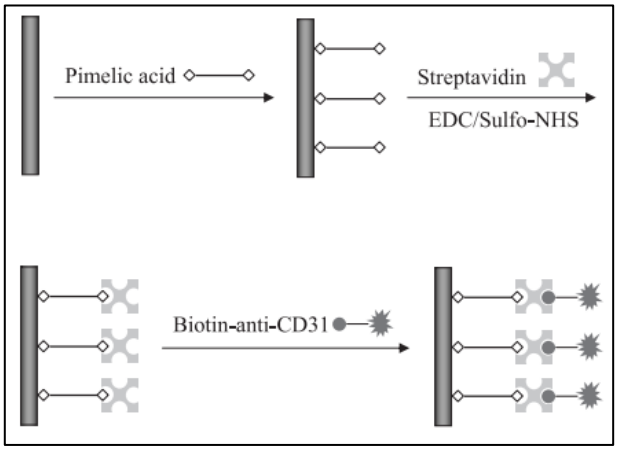

Figure 1-1: Illustration of the Functionalization of Ni Nanowires.

Ni nanowires functionalization by pimelic acid linker that bound streptavidin proteins. Streptavidin proteins have high affinity for biotin molecules, which allows them bounds to biotinylated antibody in order to target the desired cells (N. Gao, Wang, & Yang, 2010).

As scientific tool, cell manipulation by magnetic NPs allows the study of cells mechanical properties and their micro-rheology. For example, magnetic nanorods (NRs) incorporated inside cells allow for magnetic deformation of intracellular structures (Castillo et al., 2014) (Figure 1-2), while rotational magnetic spectroscopy allows for measuring viscoelastic properties of living cells by using magnetic microwires (Berret, 2016), and nuclei using magnetic NRs (Celedon, Hale, & Wirtz, 2011).

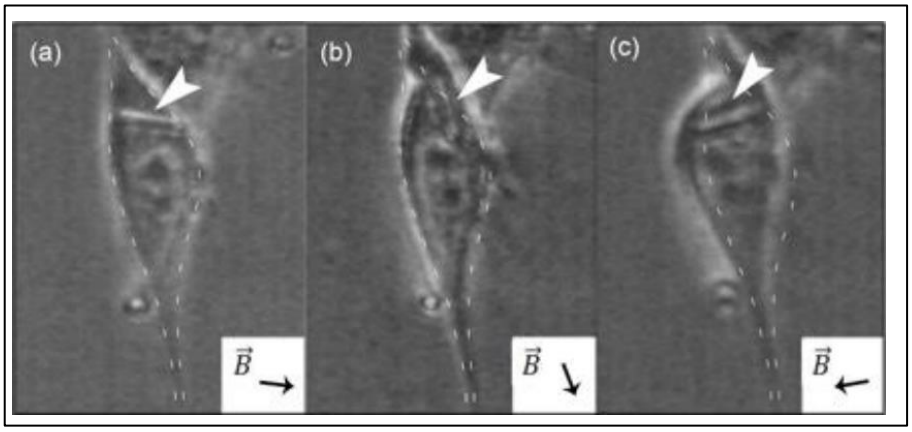

Figure 1-2: Ni-Pt Nanorods Deforming a Living Cell.

NIH/3T3 cells that had incorporated Ni-Pt nanorods that are deformed when an external magnetic field is applied (Castillo et al., 2014).

As a diagnostic tool, cell manipulation by magnetic NPs can be used to obtain magnetic resonance images to detect tumors and monitoring cell migration (Bulte, 2005) (Figure 1-3). Also, magnetic NPs can be used to study isolated cells and cells components by magnetic sorting (Hultgren et al., 2008; Perrin-Cocon, Marche, & Villiers, 1999) (Figure 1-4).

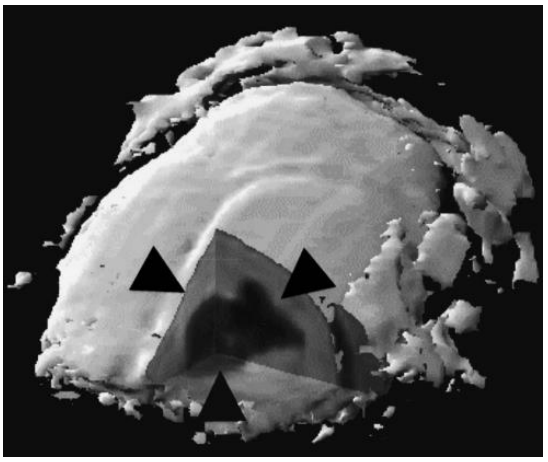

Figure 1-3: 3D Reconstructed *in vivo* Magnetic Resonance Image.

Rat brain showing distribution of magnetically tagged cell at 6 weeks after transplantation, which has migrated from the ventricle into the parenchyma (arrowheads) (Bulte, 2005).

Figure 1-4: Magnetically Isolated Endocytic Compartment.

Electron microscopy of U937 cells that were incubated with micro-beads and magnetically fractionated. Bar = 0.1 μm (Perrin-Cocon et al., 1999).

As treatment tool, cell manipulation allows controlling cell behavior. For example, osteogenesis differentiation of bone marrow mesenchymal stem cells can be achieved by cell culture on a magnetic NP composite scaffolds when a pulsed electromagnetic field is applied (Huang et al., 2017). Another example is cell death , which can be triggered by drug-carrying magnetic NP when implanted in blood vessels and magnetic guidance to the target site (Hournkumnuard & Natenapit, 2013), as well as by NPs rotation inside target cells, producing thermal or mechanical damage.

Thermal damage is generated by high temperatures (hyperthermia) caused by the rotation of magnetic spherical particles (Figure 1-5) inside cells due to the application of high-frequency MF. *In vitro* studies of such treatments have shown the ability to decrease the viability of carcinoma cells (Figure 1-6) (Liao et al., 2015) without affecting other cells, effect that depends on the cell line (Fukao et al., 2000).

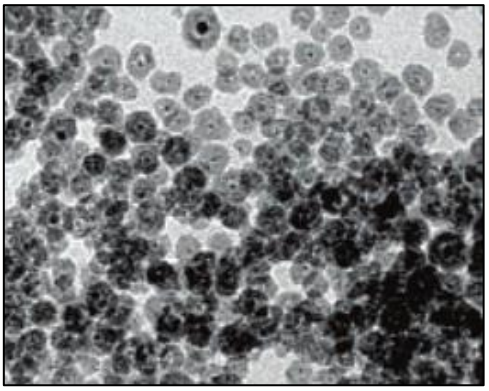

Figure 1-5: Nanospheres.

FePt@CoS2 yolk-shell nanocrystals (J. Gao et al., 2007).

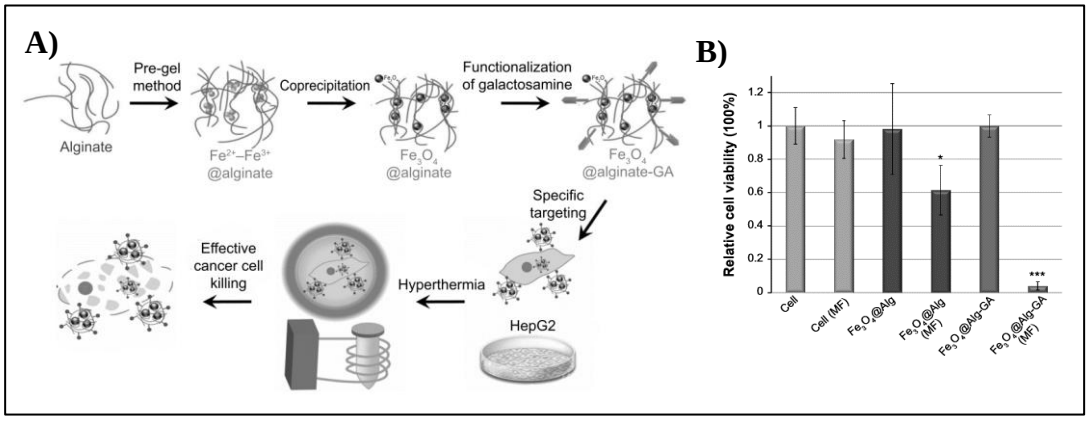

Figure 1-6: Magnetic Nanoparticle Synthesis and Treated Cell Viability.

A) Fe_3O_4@Alginate-Galactosamine nanoparticles for magnetic fluid hyperthermia. **B)** Viability of HepG2 cells incubated with nanoparticles and magnetic field. Groups treated with magnetic nanoparticles, functionalized with galactosamine to target cells and subjected to magnetic fields, show the lower viability (Liao et al., 2015).

Mechanical damage is achieved by forces produced from nanocylindrical magnetic particles (Figure 1-7) that rotates at low-frequency by an external MF and can lead to cell death (Figure 1-8) (Fung, Kapadia, Pierstorff, Ho, & Chen, 2008).

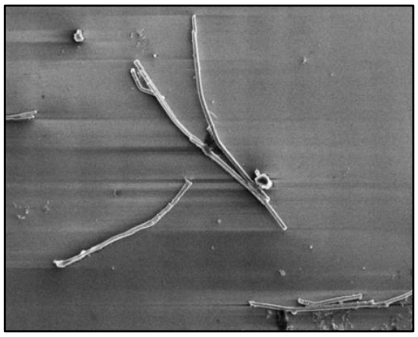

Figure 1-7: Nanocylinders.

Ni nanowires (Prina-Mello, Diao, & Coey, 2006).

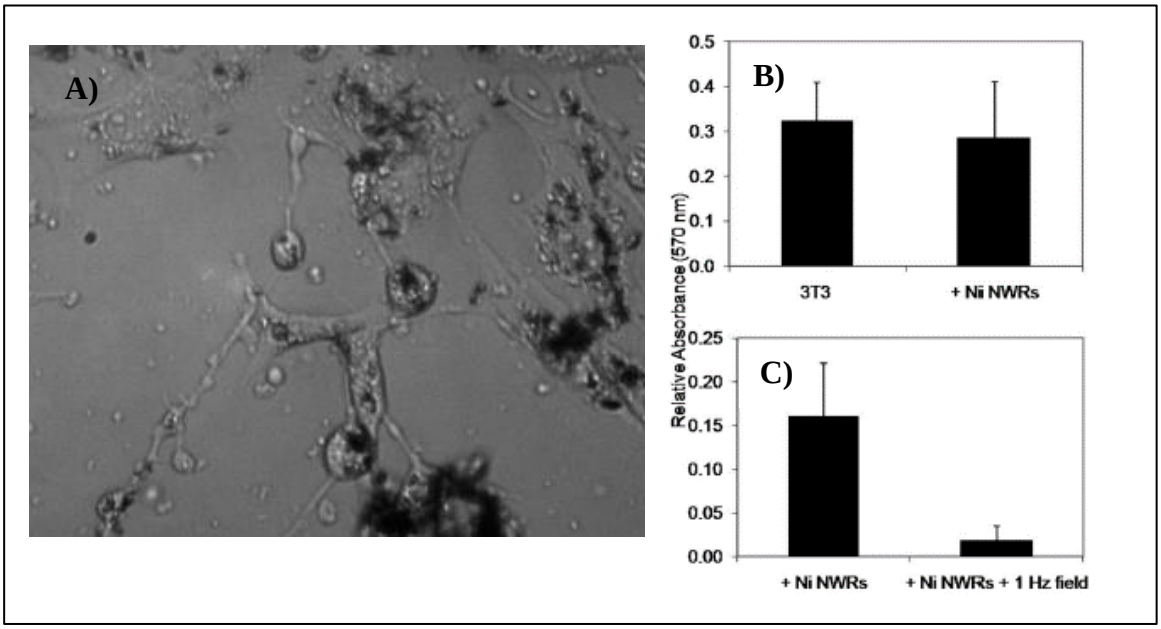

Figure 1-8: Nanorods Magnetically Rotated inside Cells and Its Effect on Viability. **A)** NIH/3T3 fibroblast cells cultured with Ni nanorods after exposure to rotating magnet of 240 mT field. **B)**, **C)** MTT assay of cells after treatment (Fung et al., 2008).

Mechanical treatment has certain advantages when compared to thermal treatment. It needs a simpler magnetic-field generating device; the rotation of NPs only affects cells that have incorporated them; and due to the fabrication technique of the cylindrical NPs, they can be made of segments of different materials, which allows the possibility of binding different molecules together, giving different properties to the same particle. However, it remains to be shown whether mechanical damage generated by NRs rotation destroy intracellular components or not, as little attention has been given to the cytoskeleton response and interaction with magnetically manipulated NRs.

Thermal and mechanical treatment produce changes in the cell behavior that can be identified by morphological changes of cell components like plasmatic membrane, cytoskeleton and nucleus, as well as proliferation inhibition. Plasmatic membrane and cytoskeleton morphological changes, as well as proliferation inhibition, indicate that certain cell functions can be impaired when treated with NPs (Pernodet et al., 2006). Membrane permeability indicates accidental cell death or late apoptosis, and nucleus condensation and fragmentation indicates apoptotic cell death. To detect cell death**,** different viability tests can be used: tetrazolium dye (MTT) detects mitochondrial activity by colorimetric analysis; terminal deoxynucleotidyl transferase dUTP nick end labeling (TUNEL) dyes fragmented DNA of apoptotic cells; fluorescent conjugated annexin V binds to membrane proteins exposed during the early stages of apoptosis; and lactate dehydrogenase (LDH) is released in the cell culture medium when cell membrane integrity is lost in death cells. However, cell response to magnetically rotated NRs inside them vary due to different reasons, such as NR composition, geometry, aggregation, concentration, application time, and target cell line (Ahamed, Akhtar, Khan, Alhadlaq, & Alrokayan, 2016; Albanese & Chan, 2011; Asharani, Xinyi, Hande, & Valiyaveettil, 2010; Elder et al., 2007; Felix, Perez, Contreras, Ravasi, & Kosel, 2016; Fung et al., 2008; Ma et al., 2014; Okuda-Shimazaki, Takaku, Kanehira, Sonezaki, & Taniguchi, 2010; Perez et al., 2016; Yamagishi et al., 2013).

1.2 Magnetic Nanoparticles

Common ferromagnetic materials used to fabricate magnetic NPs are Ni, Fe and Co, all of which are able to respond to applied MFs. Ferromagnetic materials can have a permanent magnetic moment in absence of external MF. When a MF is applied ($\vec{B}$) their magnetic momentum tends to align to its direction ($\vec{M}$). Since Ni has a lower magnetization than Fe and Co (Gong, Li, Zhao, & Chen, 1991), it is commonly chosen to fabricate magnetic NPs aiming to minimize magnetic aggregation. However, Ni NPs requiring long sonication times to ensure its dispersion before being added to a cell culture (Byrne et al., 2009; Contreras, Sougrat, Zaher, Ravasi, & Kosel, 2015; N. Gao et al., 2010; Perez et al., 2016; Prina-Mello et al., 2006).

It has been observed that dispersed Ni NWs added to cell culture are internalized by cells in vesicles (Felix et al., 2016) (Figure 1-9), via the integrin-mediated phagocytosis pathway (Hultgren et al., 2008), triggering lysosome reorganization around the nucleus (Prina-Mello et al., 2006). Incorporated NWs locate in late endosomal/lysosomal compartments or dispersed in the cytosol (Safi et al., 2011).

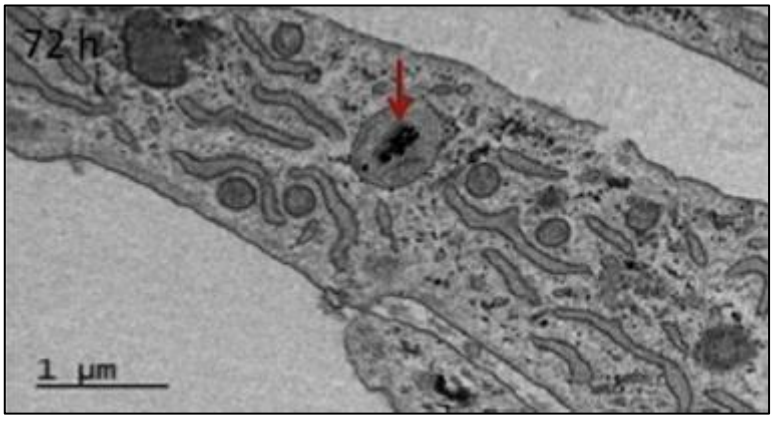

Figure 1-9: Ni Nanowires Internalized in Cells inside Vesicles.

Electron microscopy images of WI-38 fibroblasts treated with Ni NWs after 72 h. Ni NWs localize inside vesicles, most likely lysosomes (red arrows). Scale bars = 1 µm (Felix et al., 2016).

Adding a paramagnetic material segment to ferromagnetic NPs, represents a novel strategy to improve its dispersion while maintaining its ability to be magnetically manipulated. This is because paramagnetic materials have weak magnetism, and therefore, less attraction occurs between the particles. Common paramagnetic materials used to fabricate NPs are Pt, Al and Ti. NPs made of these materials form stable colloidal systems since its zeta potential magnitude are higher than +25 mV or smaller than -25 mV (Azouri et al., 2006; Beyribey, Çorbacioğlu, & Altin, 2009; Li, Aldayel, & Cui, 2014), thus they are more easily dispersed that particles that have zeta potential values closer to 0 mV. These paramagnetic materials have shown certain levels of cytotoxicity (Bahadar, Maqbool, Niaz, & Abdollahi, 2016), however, Pt NPs are of particular interest since it shows selective toxicity to cancer cells

(Bendale, Bendale, & Paul, 2017). For example, Pt segment has been used to fabricate Ni-Pt composite NRs that shows to be easily dispersed in order to be applied to cell culture, and maintaining its ability to rotate inside cells to deform them when exposed to 300 mT MF (Castillo et al., 2014). However, to the date, the biological response of cells that have incorporated Ni-Pt composite NRs, as well the underlying mechanisms of cell death with magnetic NRs rotation, remain understudied.

1.3 Ni and Pt Nanoparticles Effect on Cells

Magnetically rotated Ni NWs *in vitro* can induce cell death. Representative works that use these methods to study Ni NPs interaction with cells are summarized in Table 1-1. Kosel and collaborators incorporated Ni NWs of 4 μm in length and 35 nm in diameter into carcinoma colorectal cells, showing that 100-500 NWs/cell generates a 34% LDH leakage after 1 h from the application of 10-30 min of 0.5 mT of alternant MF (Contreras et al., 2015). Rozhkova, Novosad and collaborators incorporated Ni microdiscs (MD) of 60 nm in length and 1 nm in diameter to glioblastoma multiform cells, showing that 10 MD/cell generates a 90% of LDH leakage after 4 h from the application of 10 min of 9 mT alternant MF (D.-H. Kim et al., 2010).

Ni NWs *in vitro*, without been magnetically manipulated, has shown dose-dependent cytotoxicity (Byrne et al., 2009; Felix et al., 2016; Perez et al., 2016). Kosel and collaborators incorporated Ni NWs of 1 μm in length and 31 nm in diameter into human fibroblast WI-38 cells, showing that 0.22 μg/mL reduced cell activity to 85%

but at concentration of 22.5 µg/mL reduced cell activity to 70%, after 72 h of NWs incorporation (Felix et al., 2016). The same group showed that Ni NWs of 5.4 µm length and 30-36 nm diameter, incorporated into human HCT 116 cells at a concentration of 10 NW/cell had not significantly reduced cell activity but at concentration of 1,000 NW/cell, cell activity was reduced to 40% after 72 h of NWs incorporation (Perez et al., 2016). Byrne and collaborators showed that Ni NWs of 20 µm in length and 200 nm in diameter incorporated into THP-1 cells at 10 NW/cell reduced cell viability to 90%, and at 500 NW/cell was reduced to 50%, after 24 h of NWs incorporation (Byrne et al., 2009). On the other hand, there are some studies that report cell uptake of Ni NWs without significant cytotoxicity (≥90% of cell viability). Reich and collaborators incorporated Ni NWs of 5-35 µm in length and 350 nm diameter into of NIH/3T3 fibroblasts, showing that the cell growth after 3 days did not change with the addition of NWs, incorporated in at least 80% of the cells (Hultgren et al., 2008). Ho, Chen and collaborators incorporated Ni NWs of 4 µm in length and 200 nm in diameter into NIH/3T3 fibroblasts cells, showing that cell activity did not change significantly with the addition of the NWs, after 12 h (Fung et al., 2008). Prina-Mello and collaborators incorporated Ni NWs of 20 µm in length and 200 nm diameter at a concentration of 10^6 NW/mL into MC3T3-E1 osteoblasts, showing >95% survival after 24 h of incubation (Prina-Mello et al., 2006). Zhang and collaborators incorporated Ni NRs of 1 µm in length and 50 nm in diameter to HeLa cells, showing that 1,000 NR/cell reduced cell activity to 90% after 24 h (Ma et al., 2014).

Table 1-1: Comparison of Ni Nanocylinders of Different Sizes Applied to Different Cells Lines.

Reference	**(Felix et al., 2016)**	**(Perez et al., 2016)**	**(Contreras, et al., 2015)**	**(Castillo et al., 2014)**	**(Ma et al., 2014)**	**(D.-H. Kim et al., 2010)**	**(Fung et al., 2008)**	**(Prina-Mello et al., 2006)**
Type	NW	NW	NW	NR	NW	Microdisc	NW	NW
Material	Ni	Ni	Ni	Pt-Ni	Ni	Fe-Ni, Gold coated and functionalized	Ni	Ni
Length	1 μm	5.4 μm	4 μm	5 μm	1 μm	1 μm	4 μm	20 μm
Diameter	31 nm	30 - 36 nm	35 nm	200 nm	50 nm	60 nm	200 nm	200 nm
Cell line	WI-38	HCT116	HCT116	NIH/3T3	HeLa	N10	NIH/3T3	MC3T3-E1
Concentration	0.22- 22.5 g/mL	10 – 1000 NW/cell	100 - 500 NW/cell	0.42 μg/mL	1000-10,000 NW/cell	10 MD/cell	-	10^6 NW/mL
Incubation time	1-3 days	1-3 days	1 h	24 h	24 h	1 h	12 h	Over night
MF	-	-	0.5 mT (alternant)	300 mT (rotatory)	-	9 mT (alternant)	240 mT (rotatory)	-
Temperature during MF	-	-	-	Environmental	-	22°C	37°C	-
Torque	-	-	$0.81 \cdot 10^{-18}$ N·m	$4.5 \cdot 10^{-15}$ N·m	-	-	$1.3 \cdot 10^{-14}$ N·m	-
Frequency	-	-	1 and 1,000 Hz (similar results)	10 Hz	-	20 Hz	1 Hz	-
MF time	-	-	10 and 30 min (similar results)	10 min (4 times)	-	10 min	20 min	-
Repose time	-	-	0 min	-	-	4 h	20 min	-
MTT	85-75% (3 days)	90-50% (3 days)	78-65%	-	90-60%	-	11%	-
TUNEL	-	-	-	-	-	60%	-	-
Annexin V	-	-	-	-	20-50%	-	-	-
LDH	-	30-90% (3 days)	34%	-	-	90%	-	-

Pt NPs cytotoxicity depends on particle size and cell line (Ahamed et al., 2016; Asharani et al., 2010; Bendale, Bendale, Natu, & Paul, 2016; Bendale et al., 2017; Elder et al., 2007; Yamagishi et al., 2013). Bendale and collaborators incorporated Pt NPs to normal peripheral blood mononucleocyte cell line and cancer human lung adenocarcinoma, ovarian teratocarcinoma and pancreatic cancer cell lines, showing that 50–200 g/mL of NPs reduces cell activity to ~60% after 48 h of incorporation, only in cancer cells. They observed both necrotic and late apoptotic cell death (Bendale et al., 2017). The same group orally administrated Pt NPs to mice *in vivo*, showing that 500-2,000 mg/kg delay lung tumor grow in a dose dependent way of 37-59% after received the treatment once daily for six weeks (Bendale et al., 2016). Elder, Yang and collaborators incorporated Pt NPs of different shapes of 11-35 nm in size to human endothelial and lung epithelial cells, showing that 0.01-500 µg/well did not generate cytotoxicity or oxidative stress after 24 h of incorporation. They also administrated 100 µg to rats by the respiratory tract, showing that the particles were retained by lung tissue with minimal inflammation, after 24 h of administration (Elder et al., 2007). Valiyaveettil and collaborators administrated intravenously Pt NPs of < 1 nm in size to mice, showing that 15 mg/kg body weight generated nephrotoxicity after 24 h of injection, but with particles of 8 nm these effects were not observed (Yamagishi et al., 2013). Ahamed and collaborators incorporated gold NRs coated in Pt of 75 nm in length and 25 nm in diameter to human breast carcinoma cells, showing that 0.1-0.8 µg/mL reduced cell activity and generates a LDH leakage in a dose dependent way, after 24 h of incorporation (Ahamed et al., 2016). Watari and collaborators incorporated Pt NPs capped with polyvinyl alcohol of 5-8 nm in size to

human lung fibroblasts cells and human glioblastoma cells, showing that 20-160 µg/mL reduced cell activity and generated micronucleations in a dose dependent way in both cell lines (Asharani et al., 2010).

Given this background, Ni-Pt composites NRs had advantageous properties to avoid aggregation, but the biological consequences of their magnetically rotation inside cells remain understudied. Therefore, the aim of this research is to determine the biological consequences of Ni-Pt composites NRs that rotate inside NIH/3T3 fibroblast cells by low-frequency rotating MF.

This thesis is organized as follows: Section 2 presents the hypothesis in which this work is based and the objectives of this work; Section 3 gives a detailed methodology for magnetic field generation device; Section 4 is the manuscript submitted to the *Journal of Nanobiotechnology*, with the main results of this thesis; Sections 5 presents the effect of experimental parameters on cell response, including methodologies, results and discussion; and Section 6 contains further discussion and the conclusions of the thesis.

2. HYPOTHESIS AND OBJETIVES

For the present research, the hypothesis is that "Ni-Pt magnetic nanorods composites that rotate at low-frequency inside NIH/3T3 fibroblast cells, generate membrane and proliferation damage" (Figure 2-1).

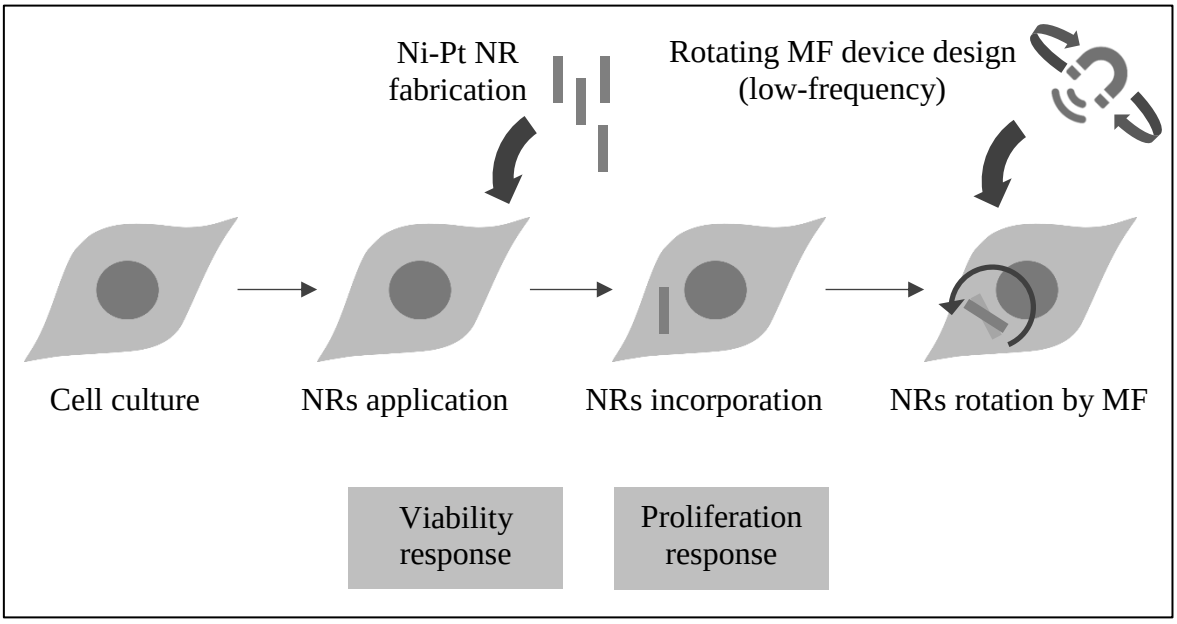

Figure 2-1: Hypothesis.

Schematic representation of the hypothesis. NR: NanoRod. MF: Magnetic Field.

In agreement with the proposed hypothesis, the general objective of this thesis is to understand the cell death and proliferation inhibition induced by the magnetic rotation of Ni-Pt NRs inside cells.

Specific objectives are: 1) To determine NRs cell proliferation inhibition when incorporated into cells; 2) To evaluate cell death caused by rotating NRs by analyzing cell permeability and nucleus morphology; and 3) To evaluate cell morphology changes caused by rotating NRs by cytoskeleton labeling.

3. MAGNETIC FIELD GENERATION DEVICE

Sample exposition to MF was made placing cell culture over two rotating magnets (Figure 3-1, A) of the MF device, or under them when observed with the optic microscope to get videos of NRs movement inside cells (Figure 3-1, B). This system was assembled to a motor, by a gear, to make the magnets rotate at 1 Hz (Figure 3-2). Further details are included in the submitted manuscript (Section 4.3.4).

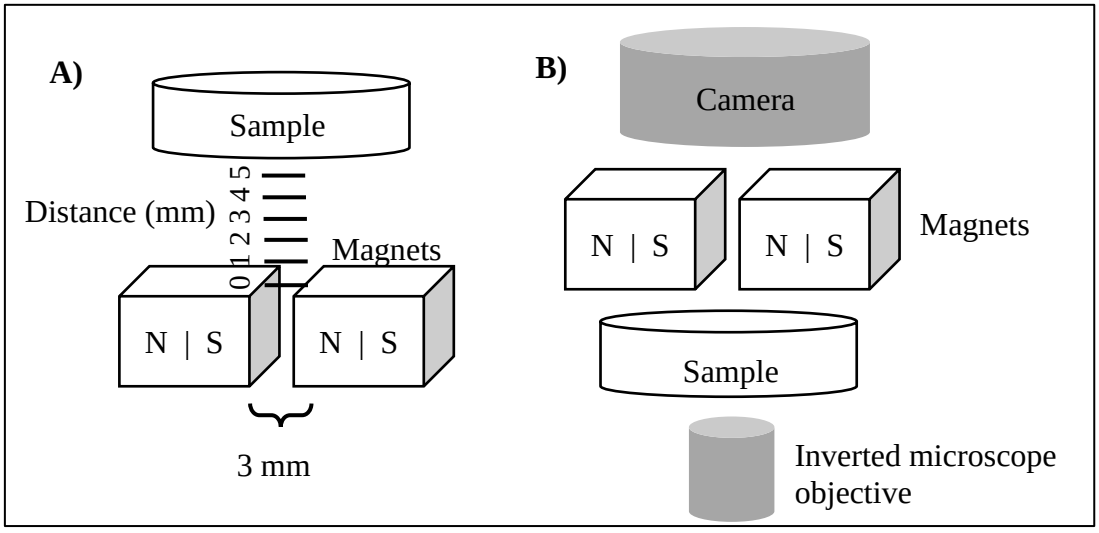

Figure 3-1: Magnetic Field Device: Sample Position.

Scheme of magnetic field device. Magnets are separated by 3 mm gap to be able to see samples under microscope. The position of the sample of both configuration of MF is shown. **A)** Magnets under the sample to make the MF treatment **B)** and over the sample to be visualized with the microscope during MF application. N and S denote the north and south poles of magnets respectively.

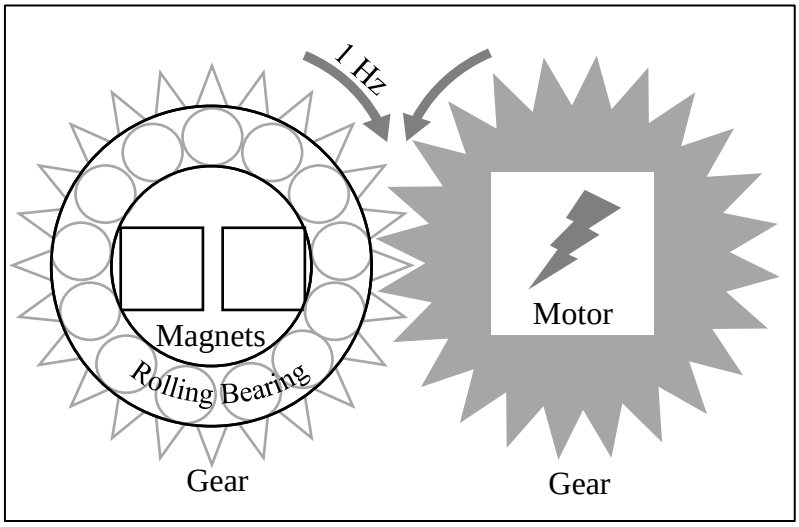

Figure 3-2: Magnetic Field Device for Controlled Rotation.

Scheme of magnetic field controlled rotation of MF device. Magnets are inside the rolling bearing. Motor rotates the magnet device at 1 Hz.

A thermal toroid was used to maintain the cell culture temperature during MF treatment. It is a fabric toroid filled with rice, which was heated to 54°C. Culture well temperature was measured after placing the thermal toroid around the culture plate. Temperature was measured for 30 minutes by a thermometer located across a perforated culture plate (Figure 3-3).

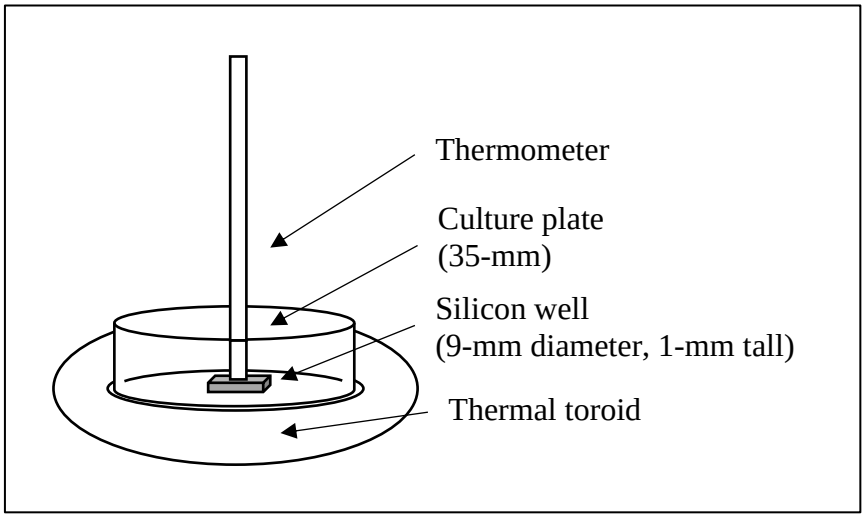

Figure 3-3: Temperature Measurement Design.

Scheme of temperature measurement system.

4. CELL MECHANICAL AND BIOLOGICAL RESPONSE TO NI-PT COMPOSITE NANORODS UNDER LOW-FREQUENCY MAGNETIC ROTATING FIELDS

Valentina B. Frenkel[1], Graciela E. Bravo[2], Hugo C. Olguín[2], Loreto M. Valenzuela[1,3,4*], Daniel E. Hurtado[3,4,5*]

* Corresponding authors: lvalenzr@ing.puc.cl; dhurtado@ing.puc.cl

4.1 Abstract

Background: Magnetic nanocylinders such as nanorods and nanowires have been inserted inside cells and mechanically manipulated by external magnetic fields in order to deform cytoplasmic structures and the cellular membrane, with the ultimate goal of inducing cell death. However, magnetic particles entirely made of ferromagnetic materials tend to aggregate before their insertion, resulting in a non-homogenous dispersion that prevents the cell uptake and increases the cytotoxic effect.

Results: We assessed the feasibility of composite Ni-Pt magnetic nanorods by studying the associated mechanical and biological consequences when inserted into cells and subject to rotating magnetic fields. Ni-Pt composite nanorods were fabricated by electrochemical deposition and characterized by Atomic Force Microscopy and Scanning Electron Microscope. They display enhanced dispersion properties, as sonication times and the aggregation effect are smaller than those

observed in single-material magnetic nanorods. Ni-Pt nanorods were effectively incorporated into the cytoplasm of NIH/3T3 fibroblast cells in culture and then subjected to low-frequency rotating magnetic field. We further confirm, using Trypan Blue dying, that such Ni-Pt nanorod magnetic treatment damages cell membrane integrity. Ni-Pt nanorods inhibit cellular proliferation after one day of adding them to cell culture.

Conclusion: The observed cell membrane integrity damage indicates a necrotic cell death. Neither the nanorod presence nor the magnetic field affected the cell membrane by itself, indicating that mechanical damage is generated by nanorods torque exerting forces on intracellular structures. Additionally, Ni-Pt nanorods presence inhibits NIH/3T3 fibroblast cell proliferation, showing a cytostatic effect.

Keywords: Magnetic nanoparticles, nanorods, NIH/3T3 fibroblasts, rotating magnetic field, cellular damage, cell death.

4.2 Background

Nanomaterials have been incorporated into cells to take advantage of their size-dependent properties (Salata, 2004). Magnetic nanomaterials have been used with the aim of externally manipulating them using a magnetic field (MF) for cell separation (Hultgren et al., 2008), sorting to purify intracellular compartments (Perrin-Cocon et al., 1999), diagnostics (Bulte, 2005), therapies as drug magnetic guidance (Senyei,

Widder, & Czerlinski, 1978), and cancer treatment by ultrasonic (Kosheleva, Lai, Chen, Hsiao, & Chen, 2016), thermal (Liao et al., 2015) or mechanical damage (Fung et al., 2008). Cell death by hyperthermia can be achieved by subjecting magnetic spherical particles to a high-frequency (kHz to MHz) rotating MF (Kossatz et al., 2015; Liao et al., 2015). Alternatively, cell death caused by mechanical damage can be achieved by applying a low-frequency (1-10 Hz) rotating MF to nanocylindrical particles such as nanowires (NWs) and nanorods (NRs) (Contreras et al., 2015; Fung et al., 2008; D.-H. Kim et al., 2010). In contrast with hyperthermia treatments, the mechanical damage induced by low-frequency rotation has the advantage of not affecting neighboring cells where NWs or NRs are absent, along with requiring a simpler MF generation system.

Nickel, iron and cobalt are the most used materials to fabricate magnetic nanoparticles (NPs), mainly due to their ferromagnetic properties, which allow them to be externally manipulated using a MF. The combination of small dimensions and high ferromagnetic properties causes aggregation, which is a common problem encountered in NPs applications (N. Gao et al., 2010; Perez et al., 2016) that hinders their incorporation into cells and enhances cytotoxic response (Albanese & Chan, 2011; Anders, Chess, Wingett, & Punnoose, 2015; Okuda-Shimazaki et al., 2010). In the attempt of preventing aggregation, Ni is frequently chosen to fabricate magnetic NPs because it exhibits a smaller remanent magnetization when compared to other ferromagnetic materials. However, sonication times required to disperse Ni NM remain large (Byrne et al., 2009; Contreras et al., 2015; N. Gao et al., 2010; Perez et

al., 2016; Prina-Mello et al., 2006). Another concern about Ni NPs is the associated cytotoxicity. While necrotic cell death can be induced by Ni NWs and MF (Contreras et al., 2015), even without MF application, Ni NPs have shown to be cytotoxic in a dose-dependent manner for human HCT-116 (Perez et al., 2016), human fibroblast WI-38 (Felix et al., 2016) and THP-1 cells (Byrne et al., 2009), but with low effect in NIH/3T3 fibroblasts (Fung et al., 2008; Hultgren et al., 2008), MC3T3-E1 osteoblasts (Prina-Mello et al., 2006) and HeLa cells (Ma et al., 2014). In conclusion, the design of a NM that allows for homogenous dispersion achieved through low sonication times, and that possesses low cytotoxic effects remains an outstanding problem that needs to be addressed before magnetic NPs can be effectively used in biomedical applications.

In a previous contribution, we have fabricated composite Ni-Pt NRs, where the paramagnetic nature of Pt has been exploited to reduce agglomeration without sacrificing size (Castillo et al., 2014). Ni-Pt NRs were introduced into NIH/3T3 fibroblasts, where we have shown that under a low-frequency rotating MF they are able to largely deform the cytoplasm and cellular membrane, but no cellular damage was assessed (Castillo et al., 2014). Therefore, the biological consequences of the application of Ni-Pt NRs and MF remain understudied. A concern about Pt NPs is their cytotoxicity, which has shown to depend on the size and the dose for human breast carcinoma, human lung fibroblasts (Asharani et al., 2010), and human glioblastoma cells (Asharani et al., 2010), but there is also evidence of Pt not being cytotoxic for blood mononucleocytes (Bendale et al., 2017), human endothelial cells

(Elder et al., 2007), and lung epithelial cells (Elder et al., 2007). The main goal of this work is, therefore, to study the biological consequences, in terms of cell proliferation and cell death, associated to mechanical damage induced by Ni-Pt NRs and the application of a low-frequency rotating MF.

4.3 Methods

4.3.1 Magnetic Nanorod Fabrication and Characterization

Ni-Pt NRs were fabricated by electrochemical deposition in the pores of anodized aluminum oxide (AAO) membranes (Whatman, Springfield Mill, Kent, UK), following the procedure described by Castillo and coworkers (Castillo et al., 2014). NRs were sonicated and suspended in ethanol (Vetec) to avoid oxidation. The resulting NR stocks were stored at room temperature. The concentration of NR stocks was calculated by counting NRs with a Neubauer chamber.

NRs were characterized using Atomic Force Microscope (AFM) (MFP-3D^{TM}, Asylum Research, Santa Barbara) analysis. To this end, NRs were mounted on metal disks using plastic solder for immobilization. To remove moisture and ethanol, samples were stored in a desiccator for 2 h. All samples were observed using AFM with air tapping mode to obtain topographic images. The calibration of the equipment considered AutoTune cantilevers type AC160TS operated at a scan rate of 0.2 to 0.05 Hz.

NRs were also characterized using a Scanning Electron Microscope (SEM) (EVO MA 10, Zeiss) with an Energy-Dispersive Spectroscopy (EDS) detector (Penta FET Precision, Oxford Instruments X-act). 10 μL of NRs dispersed in ethanol were sonicated for 3 s with an ultrasonic cleaner (CD-2800, Boque Bystems), mounted on a Sn-Si substrate, and then air dried for 20 minutes, before acquiring SEM images and analyzing the sample composition with EDS (EHT = 20 kV, WD = 8.5 mm). NRs size was calculated from SEM images of four NRs and from AFM measurement of 8 NRs.

4.3.2 Nanorod Incorporation into Cell Culture

NIH/3T3 mouse embryo fibroblasts were maintained in high-glucose Dulbecco's Modified Eagle Medium (DMEM) (CellGro - Mediatech) supplemented with 10% of fetal bovine serum (FBS) (CellGro - Mediatech) and 1% of penicillin/streptomycin (CellGro - Mediatech). Cells were kept at 37°C and 5% CO_2 in a humidified incubator in a 35-mm cell culture plate to a confluence of 50%. Silicone isolator wells of 9 mm diameter and 1 mm deep (Invitrogen) were used on a 5-mL plate to seed cells at a density of 3,100 cell/cm^2.

Ni-Pt composite NRs were added to cell culture 24 h after seeding cells into the silicone isolator wells by changing the culture medium for 90 μL of a solution of Ni-Pt NRs at a concentration of 100 NRs per seeded cell. NRs solution was prepared like described before, replacing ethanol for culture medium and sonicating 3 seconds to

avoid the aggregation of NRs before adding them to cell culture. Aggregation was assessed by measuring the surface area of each aggregate using ImageJ 1.50b software (Schneider, Rasband, & Eliceiri, 2012).

To confirm that Ni-Pt composite NRs were incorporated in cells, samples were analyzed after 24 h of NRs addition. A rotating MF was applied to cells, and the interaction was monitored in real time by an inverted optical microscope (CKX41, Olympus) equipped with a camera (Q-Color 3, Olympus) using the microscope software (Q-Capture 7.0.4324.5). Additionally, cells were exposed to trypsin-EDTA 1X (CellGro - Mediatech) to detach them from the plate substrate and images were taken with the optic microscope. The localization of NRs and the released cells in the same plane indicated that NRs were inside cells.

4.3.3 Magnetic Field and NRs Manipulation inside Cells

To generate a MF of 360 mT, two neodymium N38 magnets (25 x 25 x 12 mm) of 530 mT were used. They were separated by a 3 mm gap to be able to manipulate NRs and have the samples available for an optical microscope at the same time (Castillo et al., 2014). This system was attached to an electric motor and rotated at 1 Hz for 30 min. For temperature control during MF application and during controls without MF, samples were covered with a hot blanket that allow maintaining the temperature to 32.7 ± 2.8°C during 30 min, to avoid thermal stress induced by environmental

temperatures that can affect cell behavior (Harding, Halevy, Yahav, & Velleman, 2016; Watanabe & Okada, 1967) and therefore minimize temperature effect.

Sample exposition to the MF was made 24 h after NRs incorporation to cell culture. Application time and frequency were different for the experiment made to analyze cell response by vital stains and the experiment that analyzes NR-cell interaction in real time under the inverted optical microscope. For vital stains, sample exposure to MF was applied for 30 min at 1 Hz, while for real time video recording MF was applied for a couple of minutes at low-frequency (≤ 1 Hz).

4.3.4 Magnetic Field Characterization

The distance between magnets and the sample was set such that the magnetic intensity at the same reached 360 mT (Figure 4-1, A), as measured by a magnetometer (524 0381, Didactic GmbH Kombi B-Sonde S, LD) connected to a sensor (531 835, Universal measuring instrument, Physics, LD). The MF intensity was measured at different locations in the plane of the samples to assess its variation from the central axis (Figure 4-1, B and C).

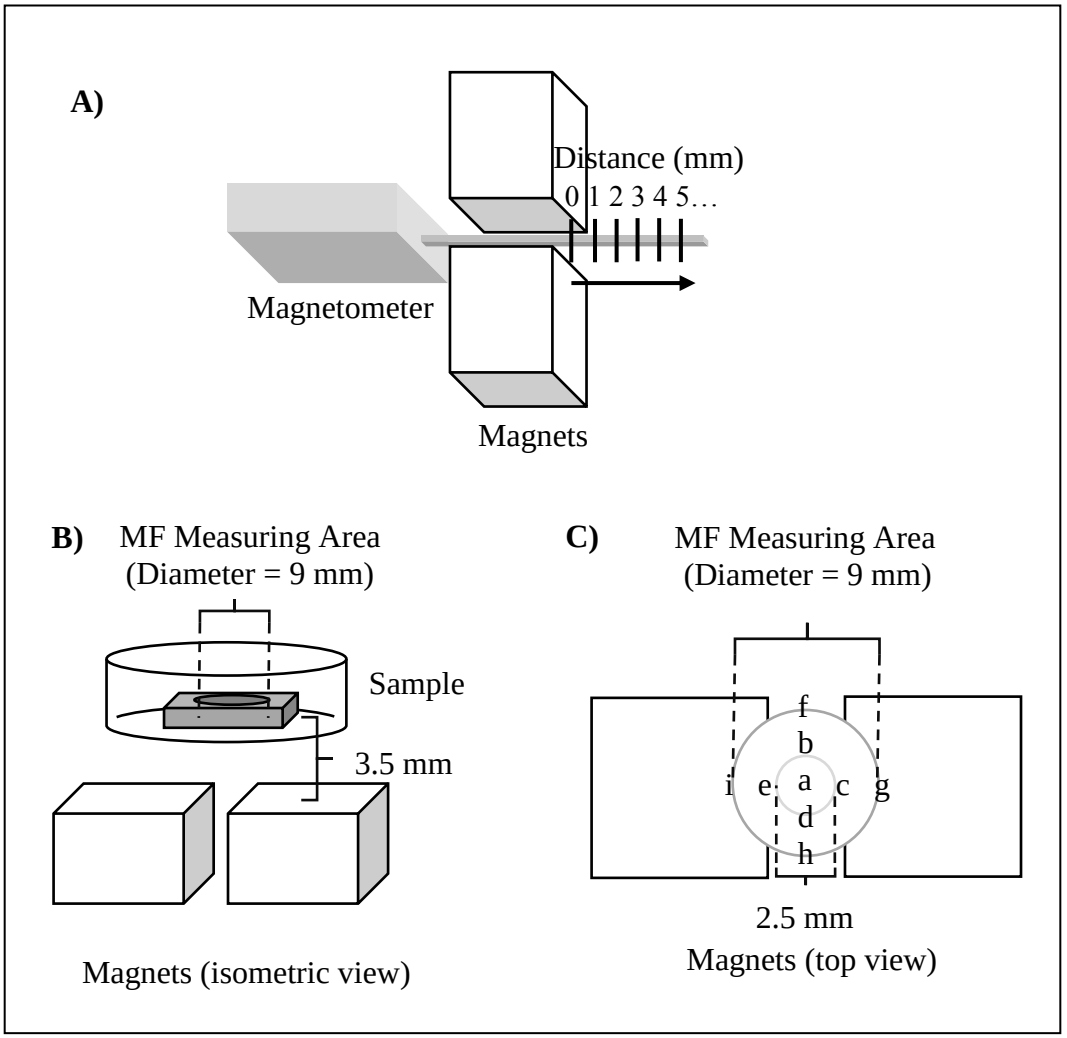

Figure 4-1: Scheme of Magnetic Field Measurement.

A) MF measurements along the central axis of the magnets were made by moving the magnetometer through the magnets. **B)** MF measurement area correspond to cell culture area (9 mm diameter) at the height at which MF was applied (3.5 mm over the magnets) **C)** top view, where the coordinates in millimeters of the points at where MF was measured are: a (0, 0); b (0, 1.25); c (1.25, 0); d (0, -1.25); e (-1.25, 0); f (0, 4.5); g (4.5, 0); h (0, -4.5); and i (-4.5, 0).

The orientation of NRs inside cells was driven by the magnetic torque ($\vec{\tau}$) generated by the rotating MF. Let ρ, L, R, and $\vec{M}$ be the density, length, radius and magnetization vector of the Ni portion of NRs, respectively. Torque was calculated using the dipolar magnetic moment ($\vec{m}$) and the MF ($\vec{B}$) vectors as follows:

$$\vec{m} = \rho\pi R^2 L\vec{M} \quad (4.1)$$

$$\vec{\tau} = \vec{m}\times\vec{B}\sin\theta \quad (4.2)$$

where θ represents the angle between $\vec{m}$ and $\vec{B}$.

4.3.5 Vital Staining with Trypan Blue and Hoechst

Cell death was assessed 20 min after the application of MF by cell staining with a Trypan Blue (TB) solution, 0.4% (Gibco - Life Technologies) for 2 min, followed by Hoechst 33342 10 µg/mL (Molecular Probes - Life Technologies) diluted 1:2,000 in high-glucose DMEM (CellGro - Mediatech) supplemented with 10% of FBS (CellGro - Mediatech) and 1% of penicillin/streptomycin (CellGro - Mediatech) for 15 min. TB stain is impermeable to healthy cells but permeable to death cells, staining them in blue, which are observable using optical microscopy. Hoechst dye emits a blue fluorescence when bound to dsDNA, making the nucleus fluorescently blue, which can be observed by fluorescent microscopy. Images were taken using an inverted optical microscope with a light source (U-RFL-T 50-100, Olympus). ImageJ 1.50b software was used to count cells. Cell viability and proliferation rate were calculated as follows:

$$Cell\ viability\ (\%) = 100\,\frac{Healthy\ cells}{Total\ cells} \quad (4.3)$$

$$Proliferation\ (\%) = 100\,\frac{Total\ cells - Seded\ cells}{Seeded\ cells} \quad (4.4)$$

where $Healthy\ cells$, cells with membrane impermeability, are the TB negatives, *Total cells* are the Hoechst positives and *Seeded cells* are the number of cells used to make the culture. Proliferation values were normalized by the mean of the control group (–NR–MF).

4.3.6 Analysis

Each experiment considered four groups: cells treated with NRs and MF (+NR+MF), cells treated with NRs alone (+NR–MF), cells treated with MF alone (–NR+MF), and a control group (–NR–MF). Experiments were repeated 6 times. Statistically significant differences between experiments were studied using a nonparametric Friedman and Dunn's multiple comparison post hoc tests with a 5% level of significance ($p < 0.05$). All statistical analyses were performed using GraphPad Prism version 7.02 for Windows (GraphPad Software, La Jolla California USA, www.graphpad.com).

4.4 Results

4.4.1 Nanorods Fabrication and Characterization

According to AFM measurements, the size of NRs was 5.01 ± 0.40 μm in length and 296 ± 17.70 nm in diameter (Figure 4-2 C and D). According to SEM measurements,

the size of NRs was 4.43 ± 0.30 µm (Ni 0.79 ± 0.08 µm, Pt 3.62 ± 0.35 µm) in length, and 255.50 nm ± 50.00 nm in diameter (Figure 4-2 A and B), thus, having an aspect ratio of 17. Diameter of each NR was 10% wider at the Ni end than at the Pt end, and both were wider than a single pore from the alumina template (200 nm) used to make the NRs, as expected (M. R. Kim, Lee, & Jang, 2010). Differences between AFM and SEM diameter measurements were expected due to microscopy differences: AFM allows to measure the height of NPs with sub-nanometric accuracy, but lateral measurements present larger differences due the tip-sample convolution and deconvolution algorithms, while SEM allows to measure lateral dimensions with nanometric accuracy (Delvallée, Feltin, Ducourtieux, Trabelsi, & Hochepied, 2015).

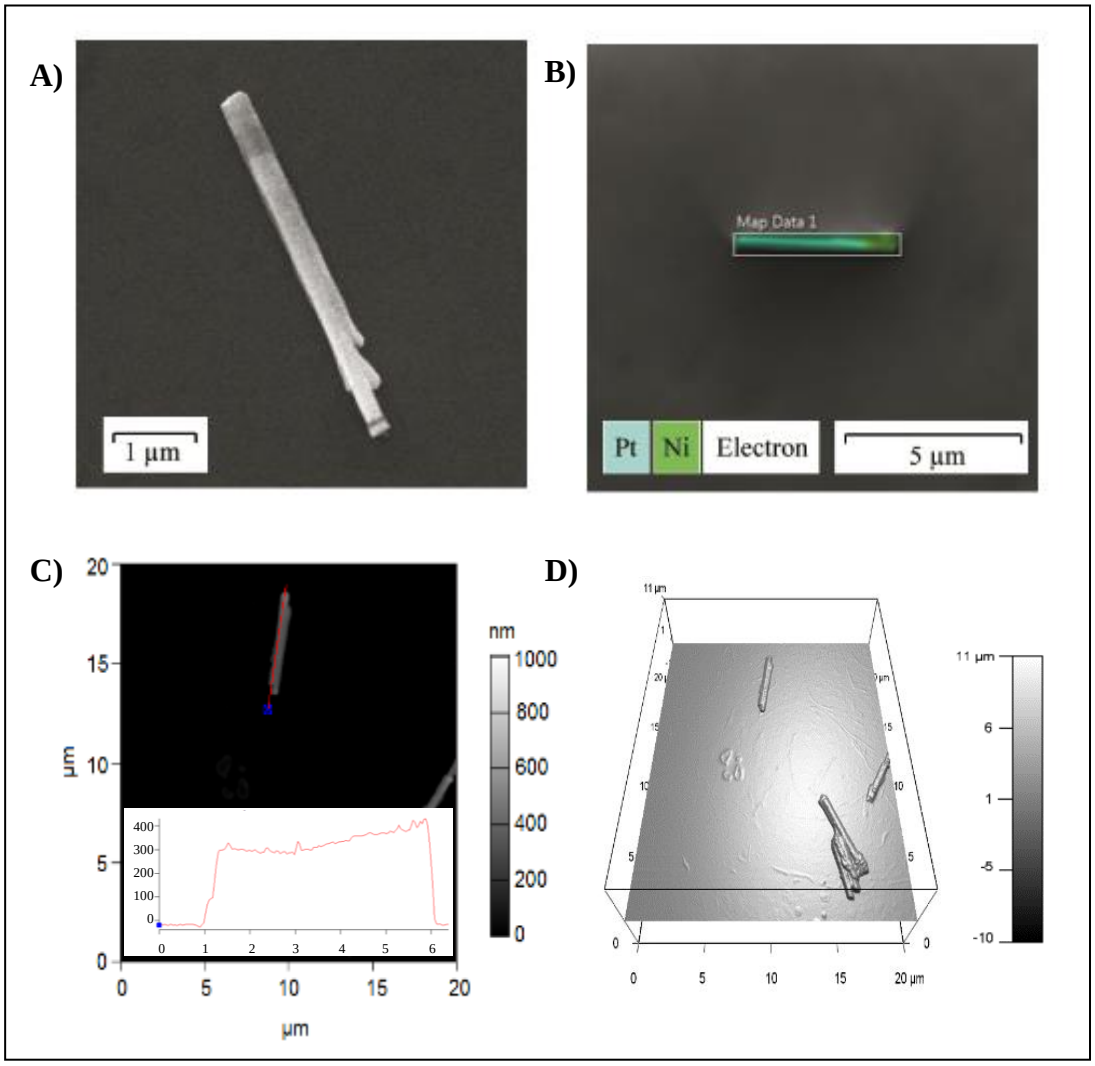

Figure 4-2: Ni-Pt Nanorods Size and Composition Characterization.

Ni-Pt NRs fabricated by electrodeposition, characterized by **A)** SEM, **B)** SEM/EDS composition analysis, which show the segments of both materials in different colors, **C)** AFM height channel topographic image with the correspondent height graph of the NR marked by the red line**,** and **D)** AFM 3D representation of height channel.

After 3 seconds of sonication, more than 50% of the aggregates had a surface area smaller than 8 μm^2 in ethanol (Figure 4-3 A and B) and smaller than 6 μm^2 in culture

medium (Figure 4-3 C and D). Aggregate surface area is used to estimate the average number of NRs in them, obtaining approximately 8 NRs per aggregation in ethanol, and 6 NRs per aggregation in the culture medium. This result is limited by the resolution of the microscope and NRs overlap.

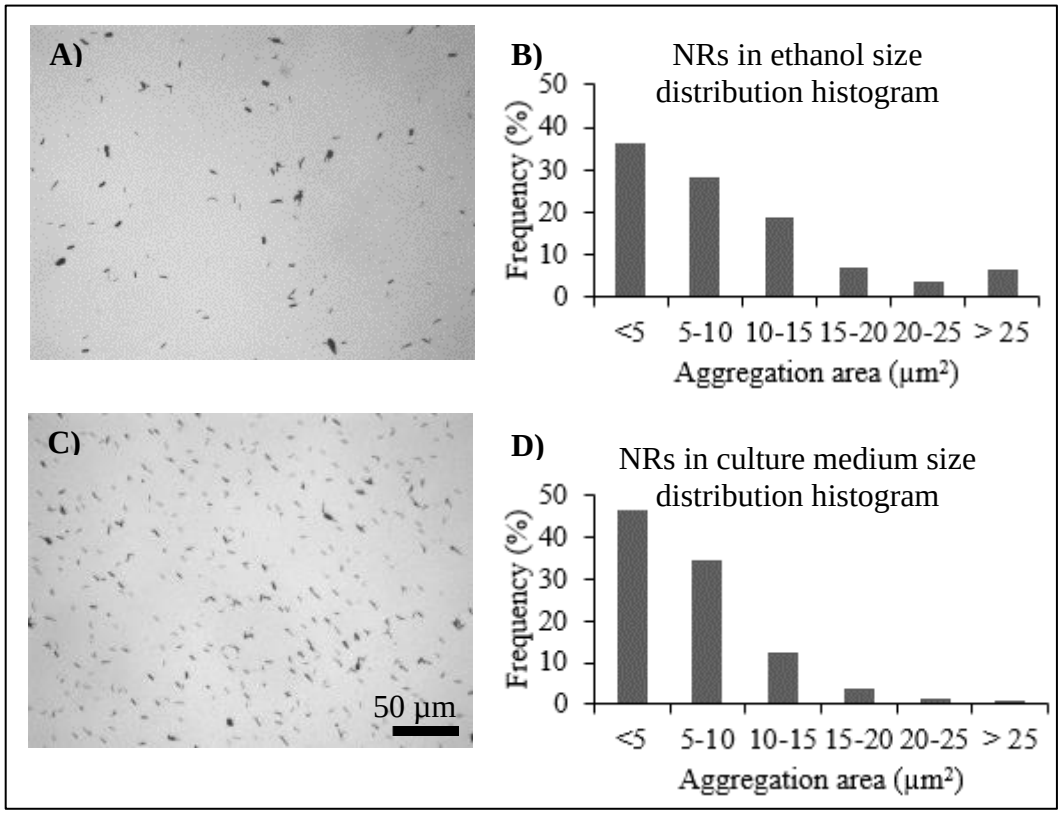

Figure 4-3: Size Distribution of Ni-Pt Nanorods Aggregates.

Appearance and size distribution of aggregates of NRs. **A), C)** Optical microscopy images at 40X and **B)**, **D)** histogram of maximum aggregates area of NRs in ethanol and in culture medium (DMEM 10% FBS 1X P/S) respectively, from the optical microscopy images.

4.4.2 Magnetic Field Characterization

The MF intensity measured along the central axis of magnets decreased as the distance from the magnets increased, starting from 754 ± 6 mT (Figure 4-4). At a distance of 3.5 mm from the magnets, the average MF applied to the cell culture well was 360 ± 50 mT, with a maximum value at its center (Figure 4-5). Maximum torque ($\theta = 90°$) of NRs subjected to the MF was $7.1 \cdot 10^{-15}$ N · m, value calculated from equations 4.1 and 4.2, considering the applied MF of 0.36 T; a Ni NR segment of $7.9 \cdot 10^{-7}$ m in length and $1.3 \cdot 10^{-7}$ m in radio, Ni density of 8,908 kg/m^3, and Ni NR magnetization of 50 A·m^2/kg (Prina-Mello et al., 2006).

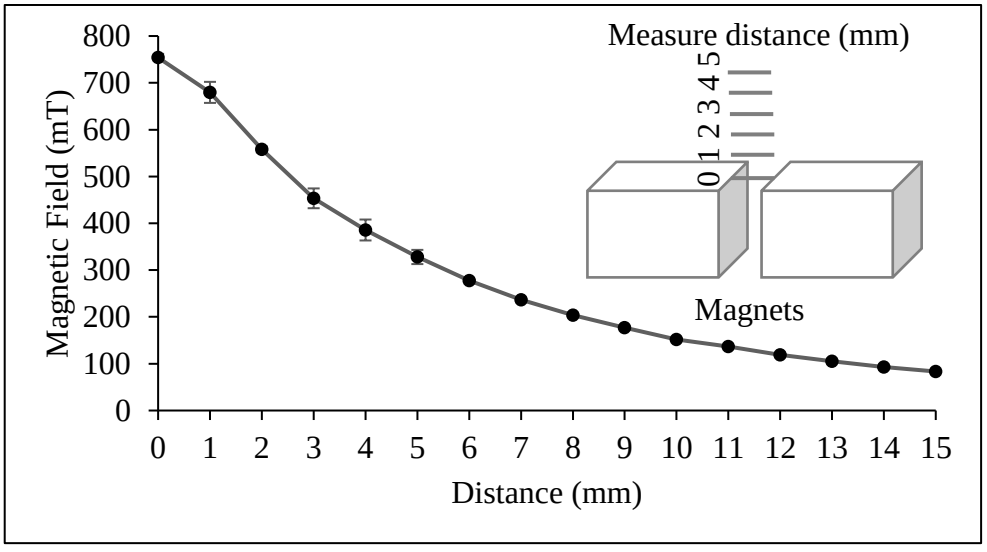

Figure 4-4: Magnetic Field along the Magnets Central Axis.

MF (mT) across the distance (mm) vertically along the central axis of the two magnets of the MF generation system. The drawing shows the magnets separated by a 3-mm gap and where the MF measure was made. Measurements were made in triplicate.

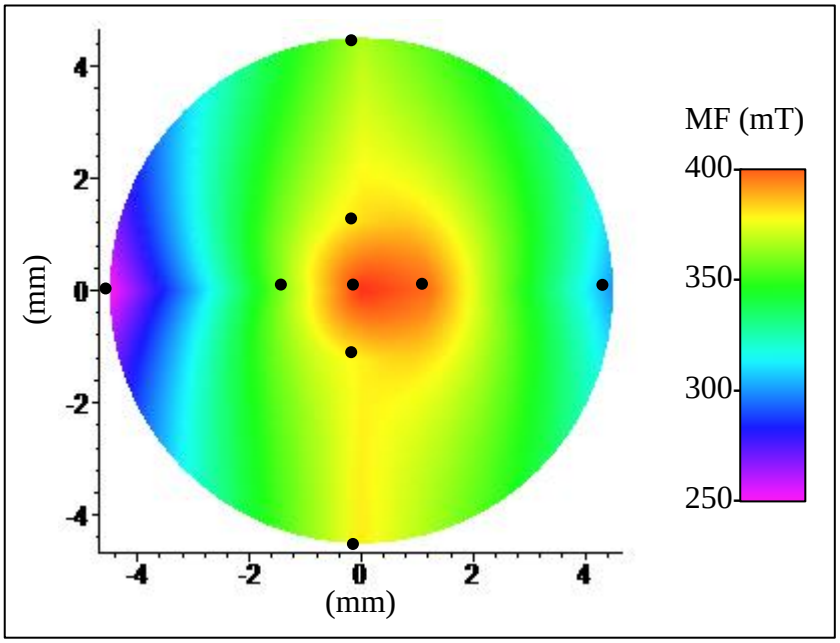

Figure 4-5: Magnetic Field at Sample Exposition Position.

MF (mT) variation with the position (mm) in the horizontal plane, at 3.5 mm of the magnet in the vertical plane. Dots indicate the position at which MF was measured, at radius of 0, 1.25 and 4.5 mm from the center.

Given the NR torque and assuming that they rotate at the center of mass located at 2 μ from the Pt end, NRs produce a force of 3.6 and 2.9 nN at the Pt and Ni ends, respectively. These forces are not enough to disrupt cell membrane, since 10–30 nN are needed to penetrate cell membrane with AFM (Hategan, Law, Kahn, & Discher, 2003) which has a smaller contact area and impacts perpendicular to cell membrane, compared with our NRs that had a larger contact area and impact cell membrane almost parallel to it. However, smaller forces of 2 pN and 12 pN can break molecular slip bonds between fibronectin and cytoskeleton (Jiang, Giannone, Critchley,

Fukumoto, & Sheetz, 2003) and change protein affinity by mechanical stretching (del Rio et al., 2009), respectively. Further, microtubules have shown 15% deformation when exposed to only 0.3 nN and at higher forces are cut (Schaap, Carrasco, de Pablo, MacKintosh, & Schmidt, 2006). Thus, while forces between 2 pN and 20 nN may do not damage membrane integrity, they can affect weaker structures such as microtubules, altering normal cell behavior.

4.4.3 Nanorods Uptake

Almost all NRs were located in apparent association with cells after 24 h of incubation, as observed from optical microscopy images (Figure 4-6). Interestingly, NRs seem to locate at perinuclear regions. In the samples analyzed, no NRs were found inside the nucleus. When applying MF, the NR inside a single cell rotates following the MF direction, without completing a full turn when it bounces back until it realigns with the MF, implying that the NR bounces against the cell membrane, which can only occur if the particle is inside the cell (Figure 4-7, Additional file 1). After cell detachment, the majority of NRs were located in apparent association with cells (81 ± 13%), been observed either in the same plane as the unattached cells or attached outside them. Remaining NRs were observed free in the cell culture plate (not associated with cells) (Figure 4-8, Additional file 2).

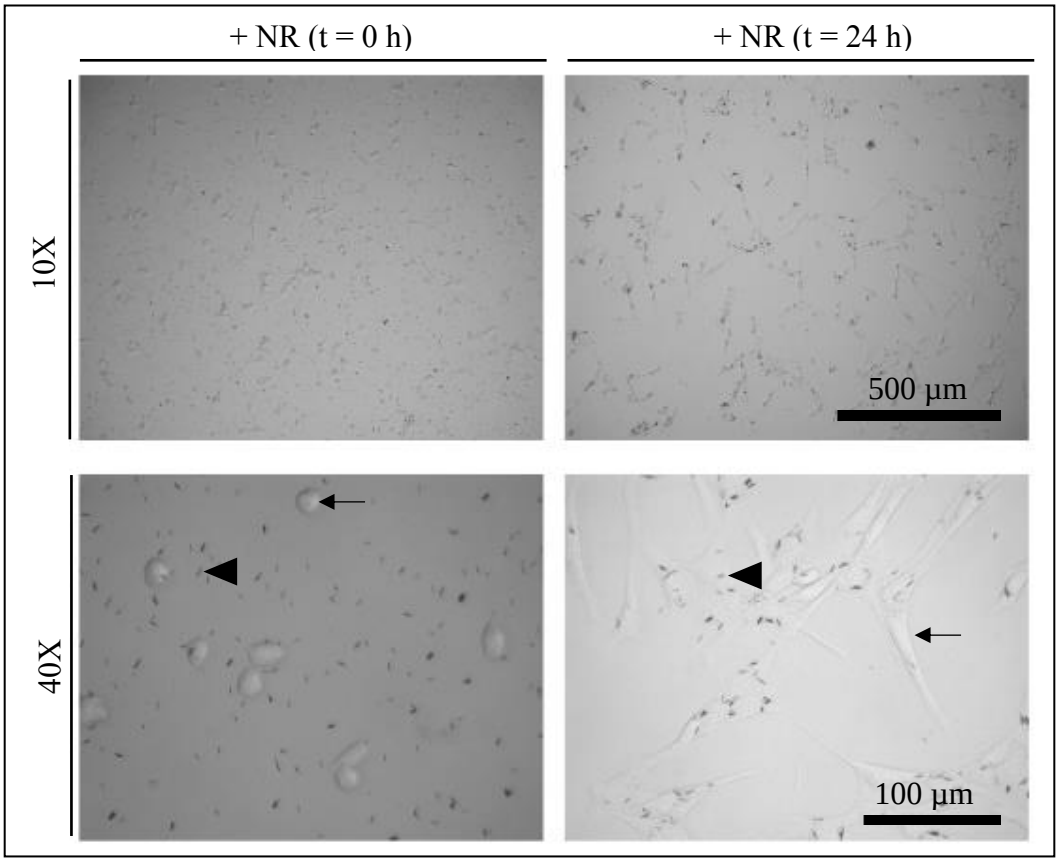

Figure 4-6: Nanorods Incorporation After 24 h.

Optical microscopy of NIH/3T3 fibroblast (arrow) with NRs (+NR) (75 NR/cell) (arrowhead) 0 and 24 h after their incorporation to NIH/3T3 cell culture. Zoom 10X and 40X.

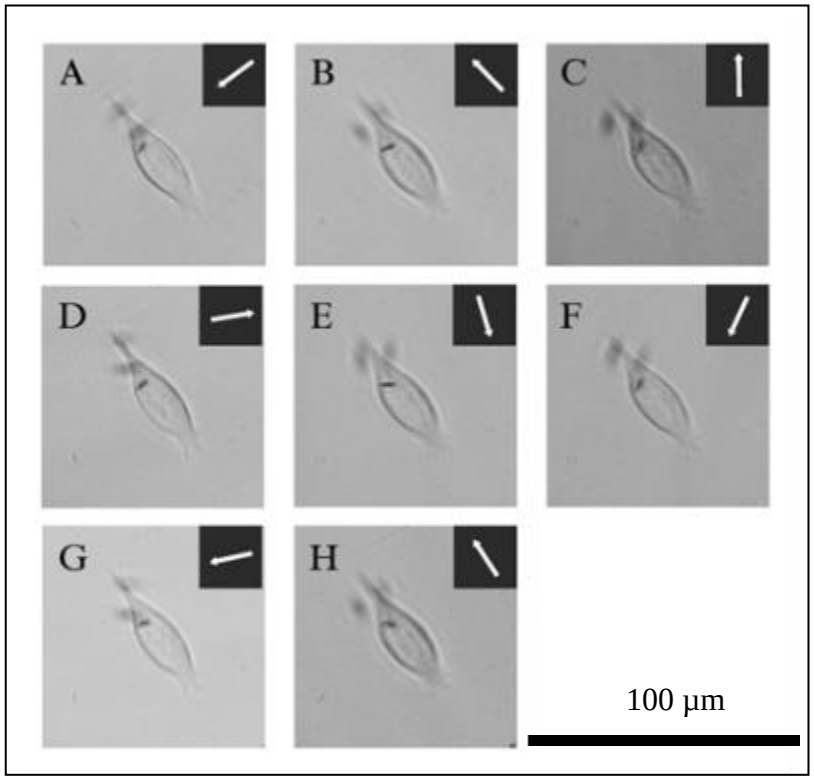

Figure 4-7: Single Nanorod Magnetically Rotated inside a Single Cell.

Optical microscopy of NR incorporated into NIH/3T3 fibroblasts cell. It is shown **A** to **H** a single cell with a single NR rotating by an external MF. MF moves clockwise and its direction is signaled by the arrow on the black square. At **B** to **C** and **E** to **F** the cylinder failed to complete the turn and returned counterclockwise to align with the field again. Finally, at **G** to **H**, the cylinder completes a turn. Zoom 20X.

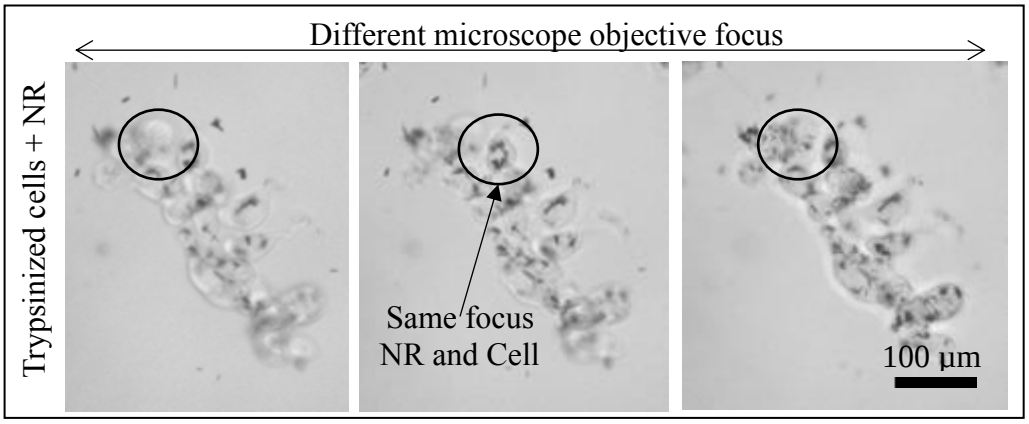

Figure 4-8: Incorporation of Nanorods inside Cells.

Optical microscopy of NR incorporated into NIH/3T3 fibroblasts cells (75 NR/cell). Images where taken after cell were treated with MF and then trypsinized. Different microscope objective focus where used a) to c), been observed at b) NRs and cells in the same focus, indicated within a circle. Zoom 20X.

4.4.4 Cellular Studies

No morphological changes were observed when incorporating NRs into cells (Figure 4-6), neither 24 h after the application of MF treatment to cells (Figure 4-9). The +NR+MF group treatment presented a significantly higher number of Trypan blue positive (+TB) cells than the other groups (Figure 4-10, A), resulting in cell viability of 88 ± 6%. This value is significantly different than that of the control ($p < 0.001$) and of the –NR+MF group ($p < 0.05$) (Figure 4-10, B).

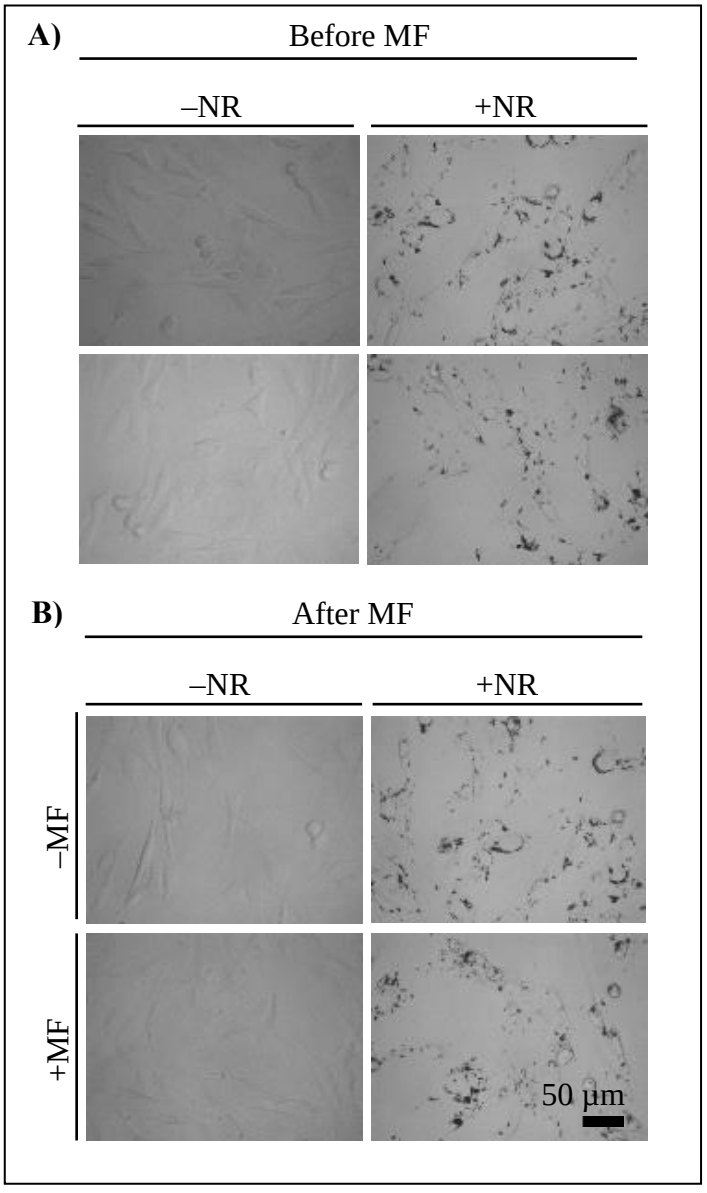

Figure 4-9: Cells Before and After Magnetic Field is Applied.

Optical microscopy NIH/3T3 fibroblasts cells with (+NR) (100 NR/cell) or without (–NR) nanorods, **A)** before and **B)** right after been treated with (+MF) or without (–MF) magnetic field. Zoom 40X.

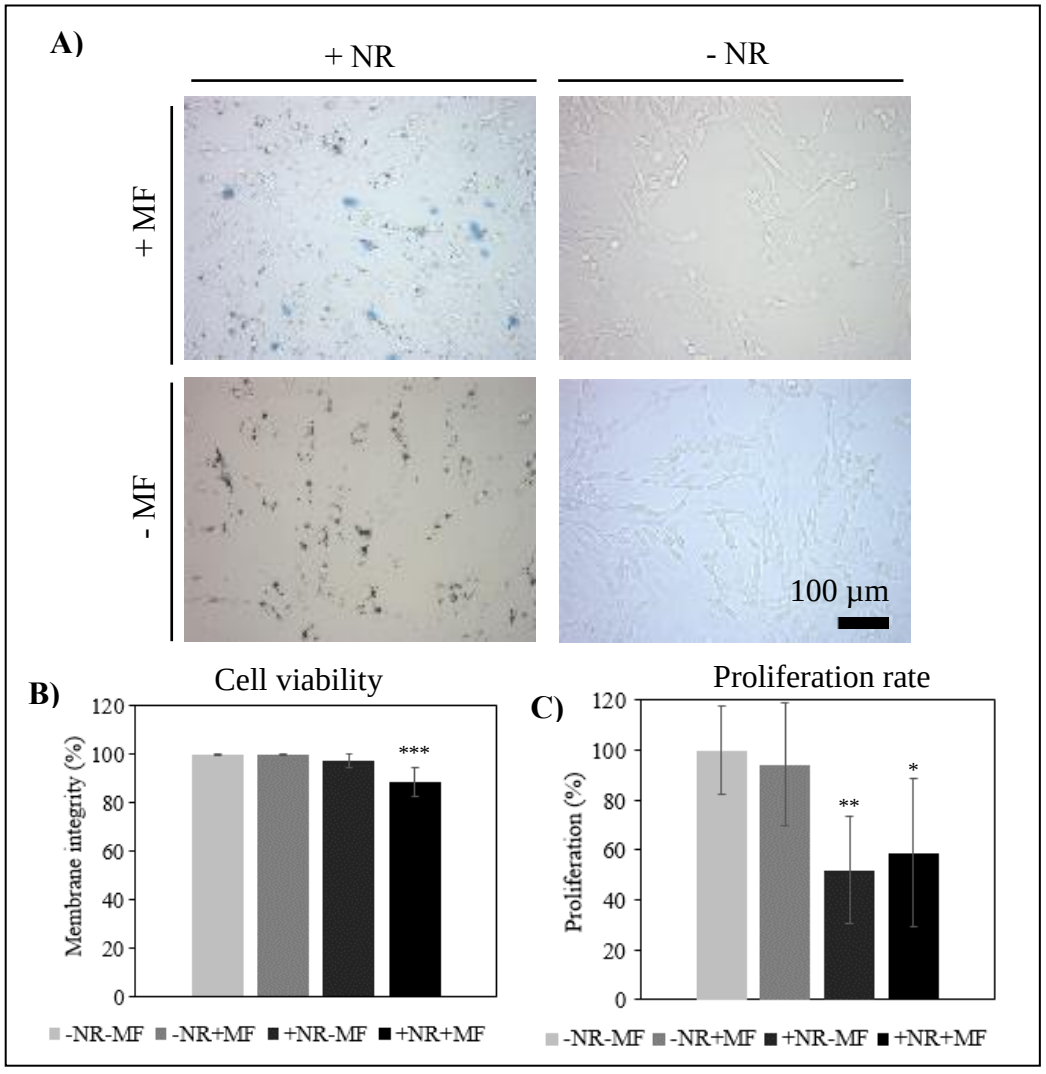

Figure 4-10: Treated Cells Viability and Proliferation Rate.

A) Optical microscopy of vital dye (TB) of NIH/3T3 fibroblasts cells with (+NR) (100 NR/cell) or without (–NR) nanorods and with (+MF) or without (–MF) magnetic field. Trypan Blue and nucleus dye was made 20 min after MF treatment was applied. Blue cells have their cell membrane integrity damaged, thus leading the dye inside. Zoom 20X. With these data was calculated **B)** cell viability by Trypan Blue and **C)** proliferation by nucleus counting. Experiments were performed six times. *$p < 0.16$, **$p < 0.05$ and ***$p < 0.001$.

The +NR+MF and +NR–MF groups displayed a significantly lower proliferation rate the control with 59 ± 29% ($p < 0.16$) and 52 ± 21% ($p < 0.05$) of proliferation rate with compared to the control, respectively (Figure 4-10, C).

4.5 Discussion

In this work, we have fabricated Ni-Pt composite NRs to use them in the treatment of NIH/3T3 fibroblasts with rotating MF. Ni-Pt NRs require 3 s sonication time to be dispersed enough to be homogenously applied to cell culture. This indicates that adding Pt to a Ni NP enhance their dispersion, since NWs made only of Ni need 2 to 60 min sonication to be dispersed before added to cell culture (Byrne et al., 2009; Contreras et al., 2015; N. Gao et al., 2010; Perez et al., 2016; Prina-Mello et al., 2006). We observed that NRs dispersion was higher when suspended in culture medium than suspended in ethanol, with less than 6 NRs per aggregation versus 8 NRs per aggregation, respectively (Figure 4-3). Previous studies showed that serum proteins, as the present on the culture medium, enhance NPs dispersion by modifying their surface (Anders et al., 2015), which explains why NRs in culture medium had fewer aggregates.

When Ni-Pt NRs were applied to cell culture and rotated at a low frequency by an external MF, we observed that the combination of NR and MF induces cell death, as revealed by the increase in membrane permeability. Cell permeability has been previously reported in gioblastoma mutiforme cells with Fe-Ni gold coated

microdiscs (D.-H. Kim et al., 2010) and in carcinoma colorectal cells with Ni NWs (Contreras et al., 2015) under alternating MF, showing cell death results from magnetically rotated NPs treatment. Thus, cell death due to NPs interaction occurs independently of the shape and material composition of the NPs. It is worth remarking that the rotation of NRs is essential to induce cell death in NIH/3T3 fibroblasts, as the introduction of NRs into cells by itself does not result in cell death (Figure 4-10, B).

Since cell membrane damage occurs in less than 30 min after treatment, we conclude that our treatment induces necrosis in roughly 12% of the cell population. This result is in contrast with the work of Ma *et al*. (Ma et al., 2014) and Perez *et al*. (Perez et al., 2016), where HeLa and HCT116 cells with magnetically rotated Ni NW of smaller dimensions than our NR, presented a necrotic death in less than 3% of cell population, for concentration levels similar to those used in our experiments. This suggests that the size, and possibly the presence of Pt, play a role in inducing necrotic death, which should be confirmed in future studies.

Cell proliferation is strongly inhibited by Ni-Pt NRs (Figure 4-10, C), a cytostatic effect that can be attributed to the material composition and size of NRs. Cell proliferation inhibition could be caused by DNA damage by generation of reactive oxygen species, and cell cycle arrest by Ni (Ma et al., 2014) or Pt (Ahamed et al., 2016) presence. Interestingly, the proliferation inhibition associated to our Ni-Pt NRs (55% proliferation rate) is in contrast with experiments using Ni NR with similar

dimensions on the same cell line (100% proliferation) (Fung et al., 2008). This observation suggests that the addition of Pt to the NR composition, rather than the size of the NR, is responsible for the cytostatic effect in NIH/3T3 fibroblasts.

Further studies should focus on the cytotoxicity of Ni-Pt NRs. Previous works have shown that Ni-Pt NRs are amenable to functionalization; Ni surface change can be achieved by oxygen reduction conditions or in acidic aqueous solution treatment (Jeon et al., 2016; S. Lee, Yoon, Choi, & Paik, 2007). This allows the Ni NPs functionalization with biomolecules, biopolymers or drugs (Kuo & Che, 2010) by bounding oxidized nickel surface of the NPs (Hurst, Payne, Qin, & Mirkin, 2006; K.-B. Lee, Park, & Mirkin, 2004) in order to improve biocompatibility, dispersion or label NPs. For example, Ni can be streptavidin coated, after pimelic acid treatment, to ligate molecules of interest that can target specific cells by biotin-streptavidin coupling (N. Gao et al., 2010); On the other hand, Pt can be amino-coated, after a wet redox procedure, to obtain positive charged particles that allow to avoid NPs aggregation (Testa, Fontana, Venditti, & Fratoddi, 2016; Wand, Bartl, Heiz, Tschurl, & Cokoja, 2016). This represents an opportunity to control the Ni-Pt composite biocompatibility as well as targeting specific cell types (Dehaini, Fang, & Zhang, 2016), while preventing aggregation of NPs, both necessary features for therapeutic applications.

Additional files

Additional file 1. Video of a cell with a NR magnetically rotating. It looks like cell membrane impedes it to complete the turn.

Additional file 2. Video of NRs in trypsinized cells. It looks like some particles are inside and outside cells, and also over the culture plate.

Abbreviations

NP: NanoParticle **NR**: NanoRod **NW**: NanoWire **MF**: Magnetic Field **Ni**: Nickel **Pt**: Platinum **SEM**: Scanning Electron Microscopy **AFM**: Atomic Force Microscopy **DMEM**: Dulbecco's Modified Eagle Medium **FBS**: Fetal Bovine Serum **TB**: Trypan Blue **LDH**: Lactate Dehydrogenase.

Author details

[1]Department of Chemical and Bioprocess Engineering, School of Engineering, Pontificia Universidad Católica de Chile, [2]Department of Cell and Molecular Biology, School of Biological Sciences, Pontificia Universidad Católica de Chile, [3]Institute for Biological and Medical Engineering, Schools of Engineering, Medicine and Biological Sciences, Pontificia Universidad Católica de Chile, [4]Center of Nanotechnology Research and Advanced Materials "CIEN -UC", [5]Department of Structural and Geotechnical Engineering, School of Engineering, Pontificia Universidad Católica de Chile, Av. Vicuña Mackenna 4860, Macul, Santiago.

Authors' contributions

VF synthesized NRs and design the MF device, GB characterized NRs by AFM. VF and GB performed all the experiments. HO supervised and guided the cell culture experiments, DH and LV (co-corresponding authors and co-PIs) supervised and guided the experimental design, analyzed data and drew conclusions. All authors participated on experimental design, discussion of the results, contributed in writing the manuscript and read and approved its final version.

Competing interests

The authors declare that they have no competing interests.

4.6 Acknowledgments

We acknowledge Pontificia Universidad Católica de Chile through grant the interdisciplinary research project CIEN-UC 3315 003 81 for its support on main materials used in this work, FONDECYT project 11121392 for optic microscope imaging, and Millennium Nucleus of Structural Biology (NuBEs), Grant P10-035-F for AFM measurements.

5. EFFECT OF EXPERIMENTAL PARAMETERS ON CELL RESPONSE DUE TO ROTATING Ni-Pt NANORODS

In addition to the experiments presented in the submitted manuscript (Section 4), we evaluated fibroblast cytoskeleton, nucleus and proliferation changes of cells under the effect of rotating Ni-Pt NRs under three different experimental settings with the objective of determining the effect of rest time after MF treatment, NRs concentration, and temperature control during MF application, in the cell response.

To our knowledge, this is the first time that Ni-Pt NRs interaction with cytoskeleton is evaluated. Cytoskeleton was chosen because of its large superficies, which make it a more probable NRs collision point compared with other cell components, and because it allows identifying morphology changes that can occur when cell functions are impaired. Also, nucleus was dying to count cells to measure cell proliferation, and to identify cell death by nuclear condensation and fragmentation.

5.1 Methods

5.1.1 Cytoskeleton Labeling

Cytoskeleton and nucleus were labeled by α-tubulin immunofluorescence and nucleus dying, respectively. Cells were washed with PBS 1X (Corning), fixed with PFA 4% (Sigma Aldrich) in PBS 1X (Corning), permeabilized with PBS 1X (Corning) 0.5% Triton-X 100 (Sigma Aldrich), blocked with PBS 1X (Corning) 3%

BSA (Merck), and labeled with murine monoclonal anti-α-tubulin antibody and donkey anti-Mouse IgG Alexa Fluor® 488 conjugate (Invitrogen- A21202). Samples were covered with fluoroshield with DAPI, histology mounting medium (Sigma Aldrich). With this technique, microtubules are green and nucleus blue, when observed under the inverted optical microscope equipped with a light source (U-RFL-T 50-100, Olympus).

5.1.2 Nanorods Rotation by the Magnetic Field

NRs and MF treatment was performed in order to analyze cytoskeleton and nucleus morphology by fluorescence labeling after the different experimental settings. Cells were incubated with Ni-Pt NRs as described in section 4.3.3, and MF treatment was administered as described in section 4.3.4. The effect of MF treatment was analyzed on cells with 15 NRs per seeded cell, that rested 24 h before cytoskeleton labeling (t = 24 h, C = 15 NR/cell, T = 33°C). Similarly, this protocol was used in experiments at different rest times (t), NRs concentrations (C) and temperatures of cell culture during MF application (T).

The effect of rest time after MF treatment was analyzed for one and 3 days, using 85 NRs per seeded cell (t = 24 and 72 h, C = 85 NR/cell, T = 33°C). Also, the effect of rest time after MF was analyzed by nucleus labeling, right after the treatment and after 3 days, using 15 NRs per seeded cell (t = 0 and 72 h, C = 15 NR/cell, T = 33°C). The effect of NR concentration was analyzed using 30, 75 and 130 NRs per seeded

cell, after 3 days of treatment (t = 72 h, C = 30, 75, 130 NR/cell, T = 33°C). Finally, the effect of temperature control during MF application was analyzed without temperature control, and with temperature control by using the thermal toroid, using 30 NRs per seeded cell in both cases (t = 72 h, C = 30 NR/cell, T = 25 and 33°C).

5.2 Results and Discussion

5.2.1 Morphological Changes in Cells Microtubules after the Controlled Magnetic Nanorods Rotation

The morphology of cells exposed to NRs is more stretched than the control group, maintaining their fibrous structure (Figure 5-1, A). This morphological change indicates that certain cell functions were impaired (Pernodet et al., 2006) by NRs, with or without MF manipulation. However, microtubule network maintains its fibrous structure after been mechanically stressed by the incorporated NRs. Since microtubules are highly dynamic polymers that are constantly polymerizing and depolymerizing, if NRs perturb them, microtubules would rapidly recover their stability (Mitchison & Kirschner, 1984). Cells with NRs, with or without MF, had a proliferation of 47 ± 16% and 54 ± 33% respectively, compared to control (Figure 5-1, B), which is consistent with the results presented in the manuscript (Section 4.4.4).

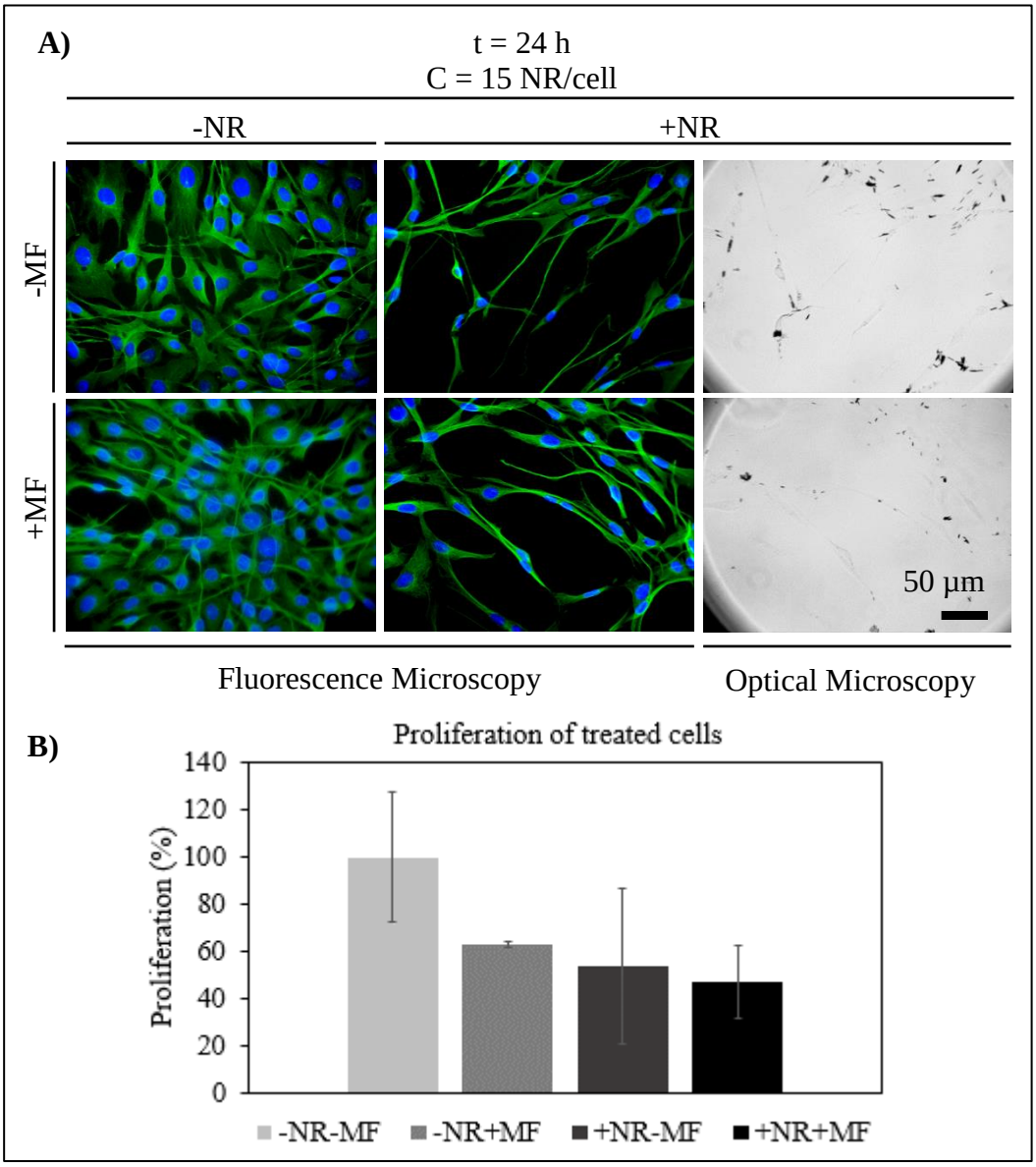

Figure 5-1: Treatment Effect in Cell Morphology and Cell Proliferation.

A) Indirect immunofluorescence of α-tubulin (green), nucleus dying (blue) and bright field of treated cells with (+NR) or without (-NR) nanorods, and with (+MF) or without (-MF) magnetic field exposition (15 NR/cell, t = 24 h, T = 33°C). Zoom 40X. **B)** Cell proliferation graph, normalized by the control group. Experiment was made with n = 4 (+NR+MF, +NR-MF, -NR-MF) and n = 2 (-NR+MF).

One experiment made under the same conditions showed lethal damage in cells exposed to rotating NRs, with presence of micronucleation (i.e., small nucleus-like fragments) and disassembling of microtubules (i.e., non-filamentous, without a fibrous structure, with the presence of non-fibrous microtubules over the plate), while the other groups cells maintain their integrity, without morphology changes (Figure 5-2). However, we were not able to reproduce this result using other stocks of cells, probably due to a genetic damage of the used cell stock. Although we were not able to reproduce this result, it is worth mentioning that under unclear conditions, a lethal mechanism occurs before 24 h of rest after MF application that involucres cytoskeleton and nucleus damage. Microtubule disassembling suggests that tubulin dimers are in the cell but not forming tubes, and then, it may be involved in the cell death. Micronucleation occurs during mitotic catastrophe, a death mechanism caused by a mitotic failure, and indicates genomic instability. Many studies have reported micronucleations as indicators of cancer susceptibility, early diagnostics of malignancy, and to predict the responsive-ness of patients on chemo- or radio-therapy (Bhatia & Kumar, 2013). Micronucleation has been reported before for Pt presence in cells (Asharani et al., 2010) and for hyperthermic cell death when damage cell components that participate in mitosis (Vidair & Dewey, 1988). Thus, our result can be provoked by a genomic instability or damage of intracellular components by magnetically rotated Ni-Pt NRs, that allowed cells to had a mitotic catastrophe death.

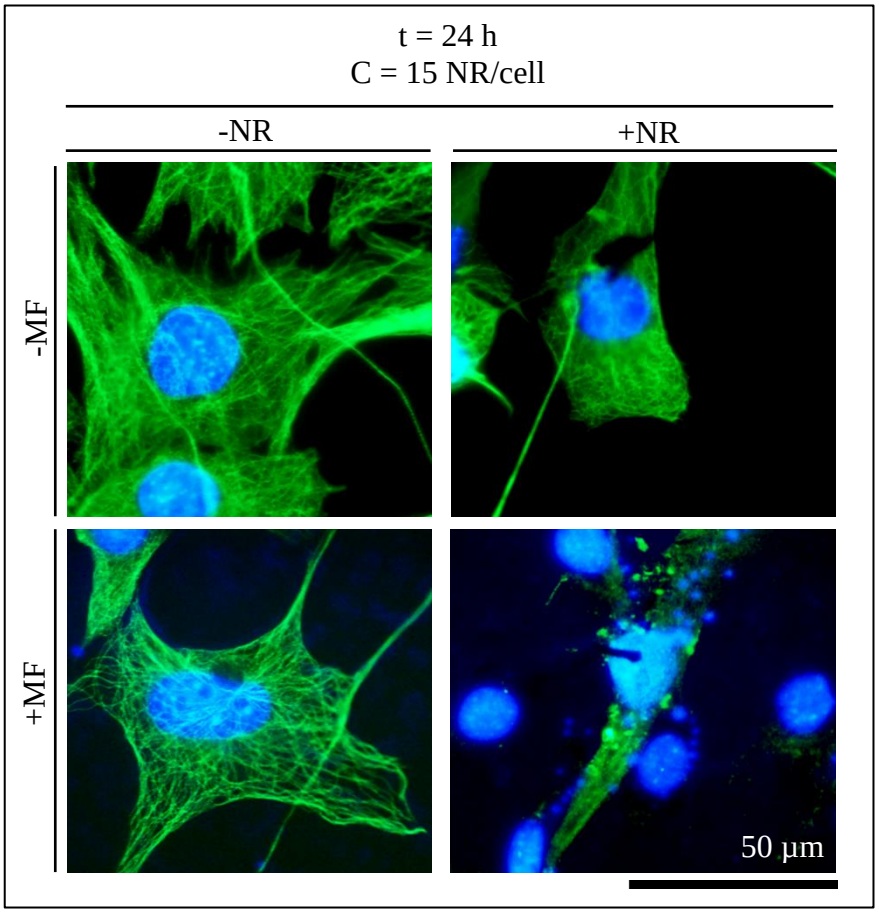

Figure 5-2: Treatment Effect in Cell Morphology.

Indirect immunofluorescence of α-tubulin (green) and nucleus dying (blue) of treated cells with cells with (+NR) or without (-NR) nanorods, and with (+MF) or without (-MF) magnetic field exposition (t = 24 h, C = 15 NR/cell, T = 33°C). Zoom 100X. Experiment was made with n = 1.

5.2.2 Effect of Rest Time after Magnetic Field Treatment

Cells exposed to NRs showed to maintain their cytoskeleton fibrous structure over time. They also changed their morphology to a stretched one after both periods, when

compared to the control group, even if MF was not applied. Interestingly, the most stretched cell morphology was observed after 24 h rather than after 72 h (Figure 5-3, A and B). However, nuclei did not show significant changes in any of the group studied, suggesting that a late apoptotic death is not occurring. Morphological changes and proliferation inhibition (Table 5-1) were time-dependent; cells with NRs had their body extended after 24 h (Figure 5-3, A), but this morphology is less distinctive after 72 h (Figure 5-3, B) compared with control cells. It could be possible that cells undergo a healing process in this period, which has to be assessed since there is no register of this in the literature. Proliferation inhibition shows to be time-dependent; cells with NRs were less confluent that cells without NRs after 24 h, and they maintain its confluence after 72 h, while cells without NRs grown normally (Figure 5-3, C). Cells with NRs were less confluent than cells without NRs after 24 h, and the inhibition was maintained after 72 h. These results suggest that Ni-Pt composites NRs presence alter cell behavior with or without the presence of an external MF in a time-dependent manner.

Table 5-1: Rest Time Effect in Cell Morphology

Analysis of cell morphology from immunofluorescence images (t = 24 and 72 h, C = 85 NR/cell, T = 33°C).

Time after MF	**Observations**
24 h	Treated samples (+NR+MF, +NR-MF, -NR+MF) proliferations are 45, 59 and 83% of control (-NR-MF) respectively. Cells with NRs (+NR+MF, +NR-MF) are and more elongated that cells without NRs (-NR+MF, -NR-MF).
72 h	Treated samples (+NR+MF, +NR-MF, -NR+MF) proliferations are 29, 38 and 92% of control (-NR-MF) respectively. Cells with NRs (+NR+MF, +NR-MF) are similar to cells without NRs (-NR+MF, -NR-MF), but slightly elongated.

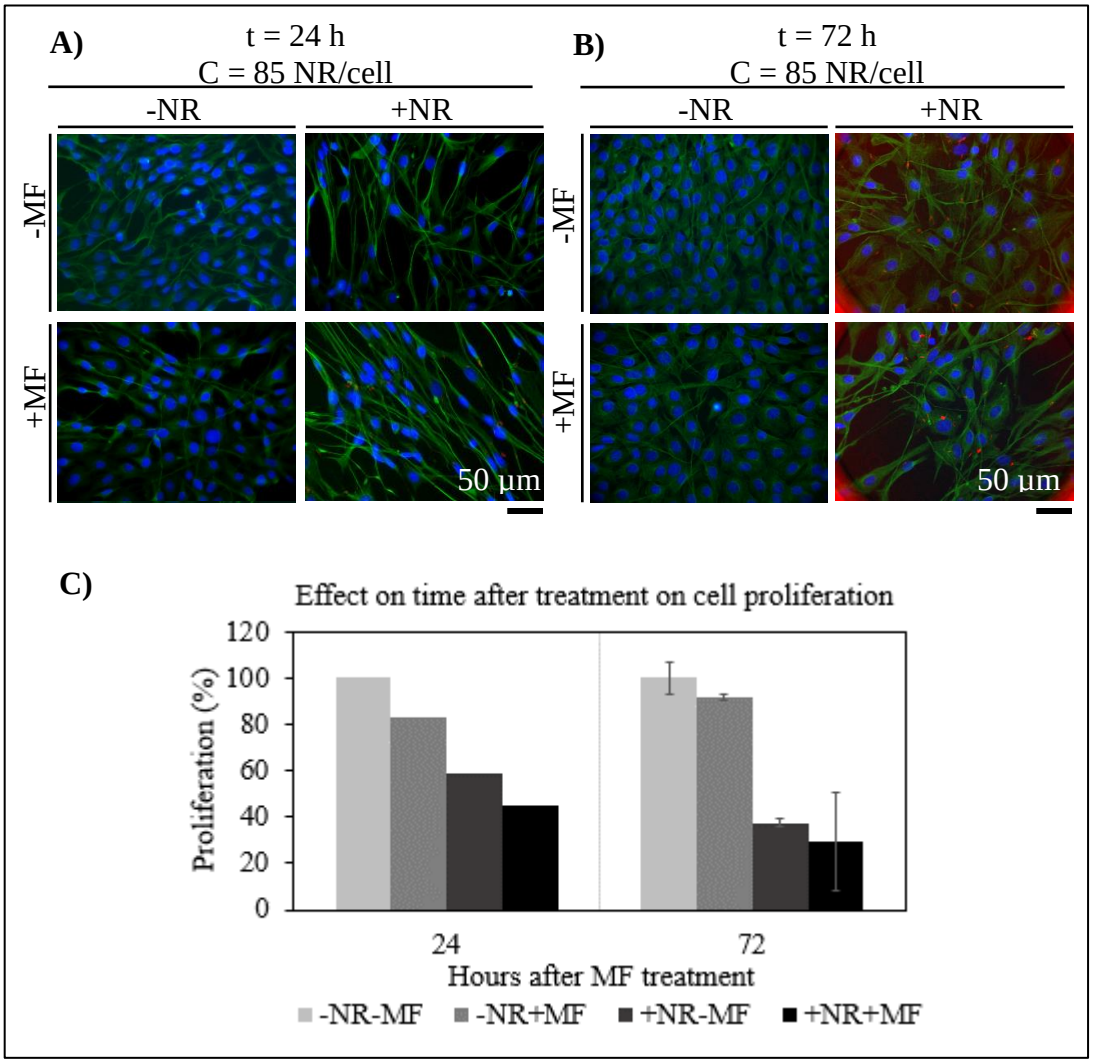

Figure 5-3: Rest Time Effect in Cell Morphology and Cell Proliferation. Indirect immunofluorescence of α-tubulin (green) and nucleus dying (blue) of treated cells with cells with (+NR) or without (-NR) nanorods, and with (+MF) or without (-MF) magnetic field exposition after **A)** one or **B)** three days of MF application (t = 24-72 h, C = 85 NRs/cell, T = 33°C). Zoom 40X. **C)** Cell proliferation graph, normalized by the control group after 72 h. Experiment was made with n = 1 (t = 24 h) and n = 2 (t = 72 h).

In one experiment, cells exposed to magnetically manipulated NRs did not lose their network appearance immediately after MF application (t=0), but at 72 h cells exposed to NRs and MF showed nuclei damage, with genetic material dispersed outside their nuclei (Table 5-2 and Figure 5-4). However, we were not able to reproduce this result, probably due to a genetic damage of the used cell stock. Thus, under unclear conditions, lethal cell damage by magnetically rotated Ni-Pt NRs occurs in a time between 0 and 72 h after MF was applied and involves nucleus disruption.

Table 5-2: Rest Time Effect in Nucleus Morphology.

Analysis of cell morphology from immunofluorescence images (t = 0 and 72 h, C = 15 NR/cell, T = 33°C).

Time after MF	**Observations**
0 h	It is observed normal nucleus morphology.
72 h	Damaged nuclei (condensed) and genetic material dispersed over the plate. Treated sample (+NR+MF) had 61% of the confluence of the control (-NR-MF) from the same period.

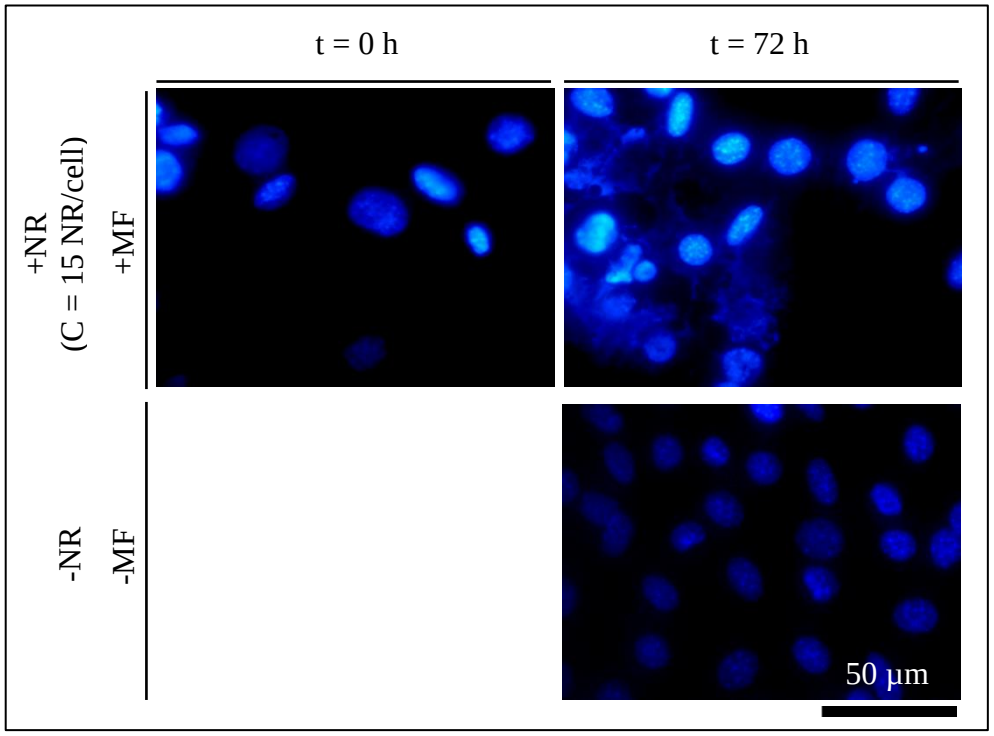

Figure 5-4: Rest Time Effect in Nucleus Morphology.

Fluorescence microscopy of nucleus dying (blue) of treated cells with (+NR) or without (-NR) nanorods, and with (+MF) or without (-MF) magnetic field exposition after **A)** one or **B)** three days of MF application (t = 0 and 72 h, C = 15 NR/cell, T = 33°C). Zoom 100X. Experiment was made with n = 1.

5.2.3 Effect of Nanorods Concentration

Cell exposed to three different NRs concentrations showed morphological changes, without losing their network appearance at any of the concentrations. At 30 and 85 NRs/cell, cell morphology almost did not change compared to control group, having at 85 NRs/cell apoptotic nuclei presence. At 130 NRs/cell, cells had an irregular morphology with a condensed nucleus (Figure 5-5), with most of the cells unattached

as an indicator of cell death. Proliferation inhibition shows to be dose dependent; cells with more NRs were less confluent that cells with less or without NRs (Figure 5-6 and Table 5-3). This result indicates not only lack of proliferation but ultimately cell death at the highest concentration (Figure 5-5), suggesting that MF treatment with Ni-Pt NRs concentration over 130 NR/cell is lethal to NIH/3T3 fibroblasts, but not at 100 NR/cell as was shown in the manuscript (Section 4).

Table 5-3: Nanorods Concentration Effect in Cell Morphology.

Analysis of cell morphology from immunofluorescence images (t = 72 h, C = 30, 85 and 130 NR/cell, T = 33°C).

NR Concentration	**Observations**
30 NR/cell	Not visible effect: treated and untreated cells look healthy. Treated samples (+NR+MF, +NR-MF, -NR+MF) proliferations are 40, 56 and 94% of control (-NR-MF) respectively.
85 NR/cell	Some cells are death, with apoptotic nucleus. Treated samples (+NR+MF, +NR-MF, -NR+MF) proliferations are 29, 37 and 91% of control (-NR-MF) respectively.
130 NR/cell	Almost all treated samples (+NR+MF) cells are death: spherical morphology and not adherent to the plate.

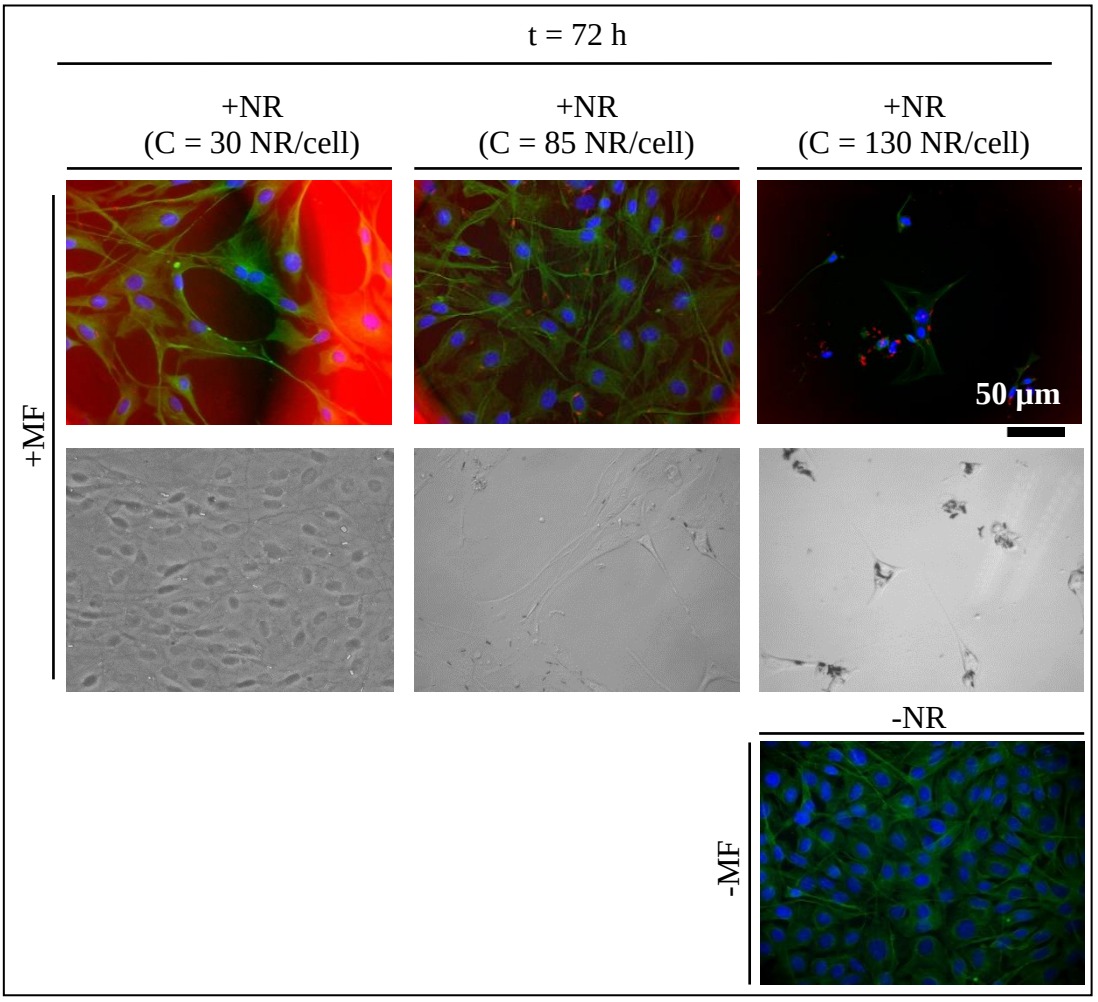

Figure 5-5: Nanorods Concentration Effect in Cell Morphology.

B) Indirect immunofluorescence of α-tubulin (green) and nucleus dying (blue) of treated cells with cells with (+NR) or without (-NR) nanorods, and with (+MF) or without (-MF) magnetic field exposition (t = 72 h, C = 31, 85 and 127 NRs/cell, T = 33°C). Zoom 40X.

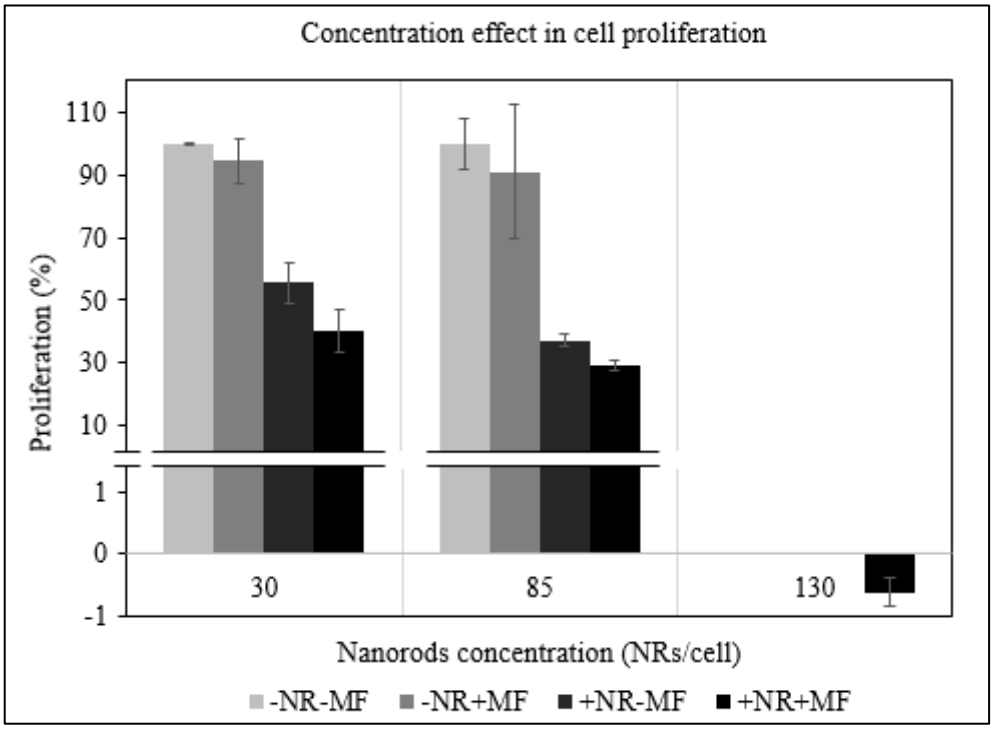

Figure 5-6: Nanorods Concentration Effect in Cell Proliferation.

Cell proliferation graph, normalized by the control group (t = 72 h, C = 31, 85 and 127 NRs/cell, T = 33°C). Experiment was made with n = 2. Only treated group (+NR+MF) was analyzed at 130 NRs/cell.

5.2.4 Effect of Temperature during Magnetic Field Treatment

Cells exposed to MF using different temperatures did not show cell morphology changes, neither viability differences between samples (Figure 5-7 and Table 5-4). This suggests that temperature, in the studied range, did not play a relevant role in the NRs mechanism when magnetically rotated inside cells (Figure 5-7, A) during a 30-min treatment. This is probably due to the short time that the cells were exposed to

lower temperatures than 37ºC. Considering that the cell replication cycle takes about 18 h, 30-min exposure to 25 and 33°C would not affect proliferation significantly.

Table 5-4: Temperature Effect in Cell Morphology.

Analysis of cell morphology from immunofluorescence images (t = 72 h, C = 30 NR/cell, T = 25 and 33°C)

Cell Culture Temperature	**Observations**
25 °C	Not morphologic difference. Both plates have all cells with not morphological changes respect to the untreated control death.
33 °C	

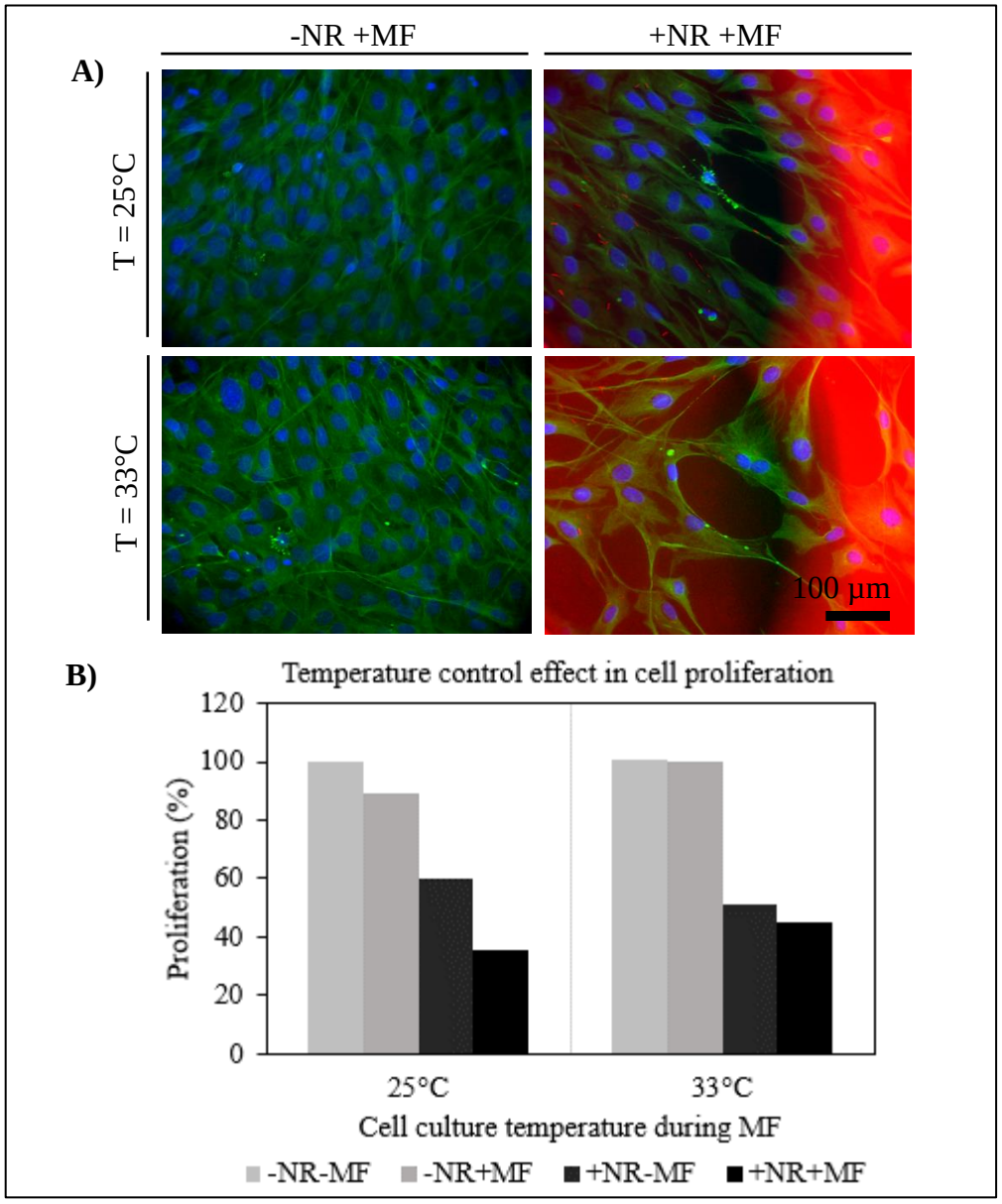

Figure 5-7: Temperature Effect in Cell Morphology and Cell Proliferation.

A) Indirect immunofluorescence of α-tubulin (green) and nucleus dying (blue) of treated cells with cells with (+NR) or without (-NR) nanorods, and with (+MF) or without (-MF) magnetic field exposition (t = 72 h, C = 30 NR/cell, T = 25 and 33°C). Nanorods are shown (red). Zoom 20X. **B)** Cell proliferation graph, normalized by the control group. Experiment was made with n = 1.

6. FURTHER DISCUSION

NIH/3T3 fibroblast cells had a preference to grow over NRs than on the culture plate without them, and incorporate them by means of vesicles, as suggested in the literature (Felix et al., 2016). We observed that most of NRs were either integrated into the cells or adhered to the cell membrane, after 24 h of adding NRs to cell culture. However, a few NRs were neither incorporated nor adhered to cell membrane, as observed after release cells from the culture plate. NRs position respect to cells may affect their effect on them, i.e.; NR located between a cell and the culture plate would have more resistance to magnetically rotate due to the presence of those two rigid surfaces; NRs located inside cells would rotate with some difficulty due to the presence of intracellular components; and NRs located over cells would rotate easily because they will not encounter the restrictions of the other two cases. NRs did not enter to the cell nucleus, so probably these cells do not have a mechanism to incorporate this NRs from the cytoplasm to the nucleus.

We observed that the 360 mT MF was large enough to rotate a single NR inside a cell. When cell cultured with NRs were subjected to MF manipulation and monitored in real time, NRs responded differently depending on their location and aggregation. For example, while free NRs rotate in the same MF direction, NRs that were apparently associated with cells rotate in irregular ways (i.e., some of them rotates without complete the turn, in what seems to be NRs bouncing against cell components, some of them attached to cell membrane rotates along the MF with one end pivoted). In aggregates, some NRs rotate with

the MF, deforming the surrounding cells, while others rotate with the MF with one extreme pivoted to the cell membrane.

Cell morphology did not change by MF nor NRs presence immediately after the treatment. MF application did not generate morphological changes in any experimental group when comparing cell appearance immediately before and after MF was applied, by optic microscopy. Thus, NRs magnetically manipulation against cells components did not affect cell adhesion.

Nuclei conserved their integrity in all experimental groups, with or without MF, probably because NRs did not have enough force to disrupt the nuclear membrane, which is stiffer and more resilient than the cell membrane (Dahl, Kahn, Wilson, & Discher, 2004), or because the magnetic manipulation of NRs generated another kind of stimulus which permeabilize cell membrane such as activating mechano-sensitive channels, as suggested in the literature (Contreras et al., 2015).

Cell proliferation inhibition by Ni-Pt composite NRs showed that they are cytostatic. Cytostaticity could be caused by Ni, Pt, or both segments of the NRs cytotoxicity, and could be produced by Ni^{2+} and/or Pt^{2+} ions release to the medium. Indeed, Ni^{2+} ions have a cytotoxic effect by damaging DNA and protein synthesis on fibroblast cells (Wataha, Hanks, & Craig, 1994), and alter gene expression by interfere with the metabolism of essential metals Fe(II), Mn(II), Ca(II), Zn(II), and Mg(II) (Kasprzak, 2003). However, it has been observed that NRs are more toxic than the equivalent amount of Ni salt, suggesting that the ion release is not the only cause of Ni NWs cytotoxicity (Felix et al.,

2016; Perez et al., 2016). On the other hand, Pt^{2+} ions could block cell division by binding to DNA, which has been observed in HeLa cells (J. Gao et al., 2007), while the Pt^{2+} effect on fibroblasts remain unknown.

7. CONCLUSIONS AND FURTHER WORK

Ni-Pt composites NRs are suitable for magnetic manipulation of intracellular structures when subject to rotating MFs. Ni allows to magnetically manipulate the particle, while Pt enhances its dispersion to achieve a homogenous NR dose per cell, improving NR cell uptake, which currently is an issue in nanotechnological therapy design. Ni-Pt NRs used in this study displayed cytostaticity, as shown in proliferation inhibition. This property can be used to eliminate malign cells if they are specifically targeted. Magnetically rotated Ni-Pt NRs inside cells provoke necrotic cell death as shown in membrane permeability. Treatment effects are dose and time dependent, but not temperature dependent during MF application.

Further studies should focus on detecting the presence of apoptotic cell death after NR magnetically rotated treatment to evaluate if it is appropriate for therapeutic applications such as cancer therapy, and on targeting Ni-Pt NRs to specific cell types as drug delivery system. For the later, cell specific target Ni-Pt NRs must be fabricated and their enhanced permeability and retention (EPR) effect *in vivo* models as well as its selective and effective accumulation in target tissues must be analyzed (Cabral, Nishiyama, & Kataoka, 2011).

BIBLIOGRAPHY

Ahamed, M., Akhtar, M. J., Khan, M. A. M., Alhadlaq, H. A., & Alrokayan, S. A. (2016). Cytotoxic response of platinum-coated gold nanorods in human breast cancer cells at very low exposure levels. *Environmental Toxicology*, *31*(11), 1344–1356. https://doi.org/10.1002/tox.22140

Albanese, A., & Chan, W. C. W. (2011). Effect of Gold Nanoparticle Aggregation on Cell Uptake and Toxicity. *ACS Nano*, *5*(7), 5478–5489. https://doi.org/10.1021/nn2007496

Anders, C. B., Chess, J. J., Wingett, D. G., & Punnoose, A. (2015). Serum Proteins Enhance Dispersion Stability and Influence the Cytotoxicity and Dosimetry of ZnO Nanoparticles in Suspension and Adherent Cancer Cell Models. *Nanoscale Research Letters*, *10*(1), 448–470. https://doi.org/10.1186/s11671-015-1158-y

Asharani, P., Xinyi, N., Hande, M. P., & Valiyaveettil, S. (2010). DNA damage and p53-mediated growth arrest in human cells treated with platinum nanoparticles. *Nanomedicine*, *5*(1), 51–64. https://doi.org/10.2217/nnm.09.85

Azouri, A., Ge, M., Xun, K., Sattler, K., Lichwa, J., & Ray, C. (2006). Zeta Potential Studies of Titanium Dioxide and Silver Nanoparticle Composites in Water-Based Colloidal Suspension. In *Multifunctional Nanocomposites* (Vol. 2006, pp. 221–223). ASME. https://doi.org/10.1115/MN2006-17072

Bahadar, H., Maqbool, F., Niaz, K., & Abdollahi, M. (2016). Toxicity of Nanoparticles and an Overview of Current Experimental Models. *Iranian Biomedical Journal*, *20*(1), 11. https://doi.org/10.7508/ibj.2016.01.001

Bendale, Y., Bendale, V., Natu, R., & Paul, S. (2016). Biosynthesized Platinum Nanoparticles Inhibit the Proliferation of Human Lung-Cancer Cells in vitro and Delay the Growth of a Human Lung-Tumor Xenograft in vivo: -In vitro and in vivo Anticancer Activity of bio-Pt NPs. *Journal of Pharmacopuncture*, *19*(2), 114–121. https://doi.org/10.3831/KPI.2016.19.012

Bendale, Y., Bendale, V., & Paul, S. (2017). Evaluation of cytotoxic activity of platinum nanoparticles against normal and cancer cells and its anticancer potential through induction of apoptosis. *Integrative Medicine Research*, *6*(2), 141–148. https://doi.org/10.1016/j.imr.2017.01.006

Berret, J.-F. (2016). Local viscoelasticity of living cells measured by rotational magnetic spectroscopy. *Nature Communications*, *7*, 10134. https://doi.org/10.1038/ncomms10134

Beyribey, B., Çorbacioğlu, B., & Altin, Z. (2009). Synthesis of platinum particles from H2PtCl6 with hydrazine as reducing agent. *Gazi University Journal of Science*, *22*(4), 351–357.

Bhatia, A., & Kumar, Y. (2013). Cancer cell micronucleus: an update on clinical and diagnostic applications. *APMIS*, *121*(7), 569–581. https://doi.org/10.1111/apm.12033

Bulte, J. W. M. (2005). Magnetic nanoparticles as markers for cellular MR imaging. *Journal of Magnetism and Magnetic Materials*, *289*, 423–427. https://doi.org/10.1016/j.jmmm.2004.11.119

Byrne, F., Prina-Mello, A., Whelan, A., Mohamed, B. M., Davies, A., Gun'ko, Y. K., … Volkov, Y. (2009). High content analysis of the biocompatibility of nickel nanowires. *Journal of Magnetism and Magnetic Materials*, *321*(10), 1341–1345. https://doi.org/10.1016/j.jmmm.2009.02.035

Cabral, H., Nishiyama, N., & Kataoka, K. (2011). Supramolecular nanodevices: From design validation to theranostic nanomedicine. *Accounts of Chemical Research*, *44*(10), 999–1008. https://doi.org/10.1021/ar200094a

Castillo, M., Ebensperger, R., Wirtz, D., Walczak, M., Hurtado, D. E., & Celedon, A. (2014). Local mechanical response of cells to the controlled rotation of magnetic nanorods. *Journal of Biomedical Materials Research. Part B, Applied Biomaterials*, *102*(8), 1779–85. https://doi.org/10.1002/jbm.b.33167

Celedon, A., Hale, C. M., & Wirtz, D. (2011). Magnetic manipulation of nanorods in the nucleus of living cells. *Biophysical Journal*, *101*(8), 1880–6. https://doi.org/10.1016/j.bpj.2011.09.008

Contreras, M., Sougrat, R., Zaher, A., Ravasi, T., & Kosel, J. (2015). Non-chemotoxic induction of cancer cell death using magnetic nanowires. *International Journal of Nanomedicine*, *10*, 2141–2153. https://doi.org/10.2147/IJN.S77081

Dahl, K. N., Kahn, S. M., Wilson, K. L., & Discher, D. E. (2004). The nuclear envelope lamina network has elasticity and a compressibility limit suggestive of a molecular shock absorber. *Journal of Cell Science*, *117*(20), 4779–4786. https://doi.org/10.1242/jcs.01357

Dehaini, D., Fang, R. H., & Zhang, L. (2016). Biomimetic strategies for targeted nanoparticle delivery. *Bioengineering & Translational Medicine*, *1*(1), 30–46. https://doi.org/10.1002/btm2.10004

del Rio, A., Perez-Jimenez, R., Liu, R., Roca-Cusachs, P., Fernandez, J. M., & Sheetz, M. P. (2009). Stretching Single Talin Rod Molecules Activates Vinculin Binding. *Science*, *323*(5914), 638–641. https://doi.org/10.1126/science.1162912

Delvallée, A., Feltin, N., Ducourtieux, S., Trabelsi, M., & Hochepied, J. F. (2015). Direct comparison of AFM and SEM measurements on the same set of nanoparticles. *Measurement Science and Technology*, *26*(8), 085601–085616. https://doi.org/10.1088/0957-0233/26/8/085601

Elder, A., Yang, H., Gwiazda, R., Teng, X., Thurston, S., He, H., & Oberdörster, G. (2007). Testing Nanomaterials of Unknown Toxicity: An Example Based on Platinum Nanoparticles of Different Shapes. *Advanced Materials*, *19*(20), 3124–3129. https://doi.org/10.1002/adma.200701962

Felix, L. P., Perez, J. E., Contreras, M. F., Ravasi, T., & Kosel, J. (2016). Cytotoxic effects of nickel nanowires in human fibroblasts. *Toxicology Reports*, *3*, 373–380. https://doi.org/10.1016/j.toxrep.2016.03.004

Fukao, H., Ikeda, M., Ichikawa, T., Inufusa, H., Okada, K., Ueshima, S., & Matsuo, O. (2000). Effect of hyperthermia on the viability and the fibrinolytic potential of human cancer cell lines. *Clinica Chimica Acta*, *296*(1–2), 17–33. https://doi.org/10.1016/S0009-8981(00)00198-4

Fung, A. O., Kapadia, V., Pierstorff, E., Ho, D., & Chen, Y. (2008). Induction of Cell Death by Magnetic Actuation of Nickel Nanowires Internalized by Fibroblasts. *The Journal of Physical Chemistry C*, *112*(39), 15085–15088. https://doi.org/10.1021/jp806187r

Gao, J., Liang, G., Zhang, B., Kuang, Y., Zhang, X., & Xu, B. (2007). FePt@CoS 2 Yolk−Shell Nanocrystals as a Potent Agent to Kill HeLa Cells. *Journal of the American Chemical Society*, *129*(5), 1428–1433. https://doi.org/10.1021/ja067785e

Gao, N., Wang, H., & Yang, E.-H. (2010). An experimental study on ferromagnetic nickel nanowires functionalized with antibodies for cell separation. *Nanotechnology*, *21*(10), 105107–105115. https://doi.org/10.1088/0957-4484/21/10/105107

Gardel, M. L., Kasza, K. E., Brangwynne, C. P., Liu, J., & Weitz, D. a. (2008). Chapter 19 Mechanical Response of Cytoskeletal Networks. *Methods in Cell Biology*, *89*(8), 487–519. https://doi.org/10.1016/S0091-679X(08)00619-5

Gong, W., Li, H., Zhao, Z., & Chen, J. (1991). Ultrafine particles of Fe, Co, and Ni ferromagnetic metals. *Journal of Applied Physics*, *69*(8), 5119–5121. https://doi.org/10.1063/1.348144

Harding, R. L., Halevy, O., Yahav, S., & Velleman, S. G. (2016). The effect of temperature on proliferation and differentiation of chicken skeletal muscle satellite cells isolated from different muscle types. *Physiol Rep*, *4*(8), 1–13. https://doi.org/10.14814/phy2.12770

Hategan, A., Law, R., Kahn, S., & Discher, D. E. (2003). Adhesively-tensed cell membranes: lysis kinetics and atomic force microscopy probing. *Biophysical Journal*, *85*(4), 2746–59. https://doi.org/10.1016/S0006-3495(03)74697-9

Hournkumnuard, K., & Natenapit, M. (2013). Magnetic drug targeting by ferromagnetic microwires implanted within blood vessels. *Medical Physics*, *40*(6), 62302. https://doi.org/10.1118/1.4805097

Huang, J., Wang, D., Chen, J., Liu, W., Duan, L., You, W., … Wang, D. (2017). Osteogenic differentiation of bone marrow mesenchymal stem cells by magnetic nanoparticle composite scaffolds under a pulsed electromagnetic field. *Saudi Pharmaceutical Journal*, *25*(4), 575–579. https://doi.org/10.1016/j.jsps.2017.04.026

Hultgren, A., Tanase, M., Felton, E. J., Bhadriraju, K., Salem, A. K., Chen, C. S., & Reich, D. H. (2008). Optimization of Yield in Magnetic Cell Separations Using Nickel Nanowires of Different Lengths. *Biotechnology Progress*, *21*(2), 509–515. https://doi.org/10.1021/bp049734w

Hurst, S. J., Payne, E. K., Qin, L., & Mirkin, C. A. (2006). Multisegmented One-Dimensional Nanorods Prepared by Hard-Template Synthetic Methods. *Angewandte Chemie International Edition*, *45*(17), 2672–2692. https://doi.org/10.1002/anie.200504025

Jeon, T.-Y., Kim, S. K., Pinna, N., Sharma, A., Park, J., Lee, S. Y., … Lee, H. H. (2016). Selective Dissolution of Surface Nickel Close to Platinum in PtNi Nanocatalyst toward Oxygen Reduction Reaction. *Chemistry of Materials*, *28*(6), 1879–1887. https://doi.org/10.1021/acs.chemmater.6b00103

Jiang, G., Giannone, G., Critchley, D. R., Fukumoto, E., & Sheetz, M. P. (2003). Two-piconewton slip bond between fibronectin and the cytoskeleton depends on talin. *Nature*, *424*(6946), 334–337. https://doi.org/10.1038/nature01805

Kasprzak, K. (2003). Nickel carcinogenesis. *Mutation Research/Fundamental and Molecular Mechanisms of Mutagenesis*, *533*(1–2), 67–97. https://doi.org/10.1016/j.mrfmmm.2003.08.021

Kim, D.-H., Rozhkova, E. A., Ulasov, I. V., Bader, S. D., Rajh, T., Lesniak, M. S., & Novosad, V. (2010). Biofunctionalized magnetic-vortex microdiscs for targeted cancer-cell destruction. *Nature Materials*, *9*(2), 165–171. https://doi.org/10.1038/nmat2591

Kim, M. R., Lee, D. K., & Jang, D. (2010). Template-Based Electrochemically Controlled Growth of Segmented Multimetal Nanorods. *Journal of Nanomaterials*, *2010*, 1–7. https://doi.org/10.1155/2010/203756

Kosheleva, O. K., Lai, T.-C., Chen, N. G., Hsiao, M., & Chen, C.-H. (2016). Selective killing of cancer cells by nanoparticle-assisted ultrasound. *Journal of Nanobiotechnology*, *14*(1), 46–57. https://doi.org/10.1186/s12951-016-0194-9

Kossatz, S., Grandke, J., Couleaud, P., Latorre, A., Aires, A., Crosbie-Staunton, K., … Hilger, I. (2015). Efficient treatment of breast cancer xenografts with multifunctionalized iron oxide nanoparticles combining magnetic hyperthermia and anti-cancer drug delivery. *Breast Cancer Research*, *17*(1), 66–83. https://doi.org/10.1186/s13058-015-0576-1

Kuo, C.-W., & Che, P. (2010). The Applications of Metallic Nanowires for Live Cell Studies. In *Electrodeposited Nanowires and their Applications* (pp. 213–228). InTech.

https://doi.org/10.5772/39482

Lee, K.-B., Park, S., & Mirkin, C. A. (2004). Multicomponent Magnetic Nanorods for Biomolecular Separations. *Angewandte Chemie International Edition*, *43*(23), 3048–3050. https://doi.org/10.1002/anie.200454088

Lee, S., Yoon, S.-M., Choi, J.-Y., & Paik, U. (2007). A new design strategy for dispersion stabilization of Ni particles based on the surface acid and base properties of Ni particles. *Journal of Colloid and Interface Science*, *312*(2), 265–271. https://doi.org/10.1016/j.jcis.2007.03.061

Li, X., Aldayel, A. M., & Cui, Z. (2014). Aluminum hydroxide nanoparticles show a stronger vaccine adjuvant activity than traditional aluminum hydroxide microparticles. *Journal of Controlled Release : Official Journal of the Controlled Release Society*, *173*, 148–57. https://doi.org/10.1016/j.jconrel.2013.10.032

Liao, S.-H., Liu, C.-H., Bastakoti, B. P., Suzuki, N., Chang, Y., Yamauchi, Y., … Wu, K. C.-W. (2015). Functionalized magnetic iron oxide/alginate core-shell nanoparticles for targeting hyperthermia. *International Journal of Nanomedicine*, *10*, 3315–3327. https://doi.org/10.2147/IJN.S68719

Ma, C., Song, M., Zhang, Y., Yan, M., Zhang, M., & Bi, H. (2014). Nickel nanowires induce cell cycle arrest and apoptosis by generation of reactive oxygen species in HeLa cells. *Toxicology Reports*, *1*, 114–121. https://doi.org/10.1016/j.toxrep.2014.04.008

Mitchison, T., & Kirschner, M. (1984). Dynamic instability of microtubule growth. *Nature*, *312*(5991), 237–242. https://doi.org/10.1038/312237a0

Okuda-Shimazaki, J., Takaku, S., Kanehira, K., Sonezaki, S., & Taniguchi, A. (2010). Effects of Titanium Dioxide Nanoparticle Aggregate Size on Gene Expression. *International Journal of Molecular Sciences*, *11*(6), 2383–2392. https://doi.org/10.3390/ijms11062383

Perez, J. E., Contreras, M. F., Vilanova, E., Felix, L. P., Margineanu, M. B., Luongo, G., … Kosel, J. (2016). Cytotoxicity and intracellular dissolution of nickel nanowires. *Nanotoxicology*, *10*(7), 871–880. https://doi.org/10.3109/17435390.2015.1132343

Pernodet, N., Fang, X., Sun, Y., Bakhtina, A., Ramakrishnan, A., Sokolov, J., … Rafailovich, M. (2006). Adverse Effects of Citrate/Gold Nanoparticles on Human Dermal Fibroblasts. *Small*, *2*(6), 766–773. https://doi.org/10.1002/smll.200500492

Perrin-Cocon, L. A., Marche, P. N., & Villiers, C. L. (1999). Purification of intracellular compartments involved in antigen processing: a new method based on magnetic sorting. *Biochemical Journal*, *338*(1), 123–130. https://doi.org/10.1042/bj3380123

Prina-Mello, A., Diao, Z., & Coey, J. (2006). Internalization of ferromagnetic nanowires by

different living cells. *Journal of Nanobiotechnology*, *4*(1), 9–20. https://doi.org/10.1186/1477-3155-4-9

Safi, M., Yan, M., Guedeau-Boudeville, M.-A., Conjeaud, H., Garnier-Thibaud, V., Boggetto, N., … Berret, J.-F. (2011). Interactions between Magnetic Nanowires and Living Cells: Uptake, Toxicity, and Degradation. *ACS Nano*, *5*(7), 5354–5364. https://doi.org/10.1021/nn201121e

Salata, O. (2004). Applications of nanoparticles in biology and medicine. *Journal of Nanobiotechnology*, *2*(1), 3–9. https://doi.org/10.1186/1477-3155-2-3

Schaap, I. A. T., Carrasco, C., de Pablo, P. J., MacKintosh, F. C., & Schmidt, C. F. (2006). Elastic response, buckling, and instability of microtubules under radial indentation. *Biophysical Journal*, *91*(4), 1521–31. https://doi.org/10.1529/biophysj.105.077826

Schneider, C. A., Rasband, W. S., & Eliceiri, K. W. (2012). NIH Image to ImageJ: 25 years of image analysis. *Nature Methods*, *9*(7), 671–5. https://doi.org/10.1038/nmeth.2089

Senyei, A., Widder, K., & Czerlinski, G. (1978). Magnetic guidance of drug-carrying microspheres. *Journal of Applied Physics*, *49*(6), 3578–3583. https://doi.org/10.1063/1.325219

Sunderland, C. J., Steiert, M., Talmadge, J. E., Derfus, A. M., & Barry, S. E. (2006). Targeted nanoparticles for detecting and treating cancer. *Drug Development Research*, *67*(1), 70–93. https://doi.org/10.1002/ddr.20069

Testa, G., Fontana, L., Venditti, I., & Fratoddi, I. (2016). Functionalized platinum nanoparticles with surface charge trigged by pH: synthesis, characterization and stability studies. *Beilstein Journal of Nanotechnology*, *7*, 1822–1828. https://doi.org/10.3762/bjnano.7.175

Vidair, C. A., & Dewey, W. C. (1988). Two Distinct Modes of Hyperthermic Cell Death. *Radiation Research*, *116*(1), 157. https://doi.org/10.2307/3577486

Wand, P., Bartl, J. D., Heiz, U., Tschurl, M., & Cokoja, M. (2016). Functionalization of small platinum nanoparticles with amines and phosphines: Ligand binding modes and particle stability. *Journal of Colloid and Interface Science*, *478*, 72–80. https://doi.org/10.1016/j.jcis.2016.06.003

Wataha, J. C., Hanks, C. T., & Craig, R. G. (1994). In Vitro effect of metal ions on cellular metabolism and the correlation between these effects and the uptake of the ions. *Journal of Biomedical Materials Research*, *28*(4), 427–433. https://doi.org/10.1002/jbm.820280404

Watanabe, I., & Okada, S. (1967). Effects of temperature on growth rate of cultured mammalian cells (L5178Y). *The Journal of Cell Biology*, *32*(2), 309–323. https://doi.org/10.1083/jcb.32.2.309

Yamagishi, Y., Watari, A., Hayata, Y., Li, X., Kondoh, M., Yoshioka, Y., … Yagi, K. (2013). Acute and chronic nephrotoxicity of platinum nanoparticles in mice. *Nanoscale Research Letters*, *8*, 1. https://doi.org/10.1186/1556-276X-8-395

APPENDIX

APPENDIX 1: PARAMETERS OF NANORODS ELECTRODEPOSITION

Electrochemical deposition was made applying negative potential according to the material. NRs length was calculated as the electric charge by the material grown rate, which defines the electrochemical deposition time. Parameters used in our Ni-Pt composite NRs fabrication are shown next.

Parameter	Value
Cupper	
Potential (V)	-0.16
Application Time (s)	817
Total Electric Charge (C)	-7.00
Platinum	
Potential (V)	-0.35
Application Time (s)	5,351
Total Electric Charge (C)	-3.77
Growth Rate (μm/C)	0.53
Theoretical Length (μm)	2.00
Nickel	
Potential (V)	-0.80
Application Time (s)	17,770
Total Electric Charge (C)	-2.86
Growth Rate (μm/C)	0.35
Theoretical Length (μm)	1.00